markedly hypoplastic. Clinodactyly was noted on the third, fourth and fifth toes on her right foot, and the third and fourth toes on her left foot. A skeletal survey did not show any radiographic bone abnormalities. Her bone age was 13–14 years and follicle-stimulating hormone was 1.57 $IU l^{-1}$ (normal range: <5 $IU l^{-1}$). Ultrasonographic examination at 16 years (before menarche), showed a hypoplastic uterus and malrotation of both kidneys. No secondary sexual characteristics were recognized until she had menarche at 17 years. Now at age of 17 years, she is still short with a height of 141 cm (−5 s.d.), weigh 31.3 kg (−3 s.d.) and OFC 50.5 cm (−4.5 s.d.). Clinical features are summarized in Supplementary Table 2.

**Structural effects of SOX11 mutations.** To determine the impact of the disease-causing mutations on human SOX11 structure and function, we mapped the mutation positions onto the crystal structure of mouse Sox4[9], that is analogous to human SOX11, and calculated free energy changes on the mutations using FoldX software[10,11]. The mutations lie in the highly conserved HMG domain, responsible for sequence-specific DNA binding (Fig. 2a)[9]. Ser60 is located in a helix of the HMG domain (Fig. 2a), therefore the S60P mutation may affect overall folding of the HMG domain and impair DNA binding of SOX11. FoldX calculations supported this prediction and the free energy change on the mutation was high enough to destabilize protein folding (>10 kcal $mol^{-1}$) (Fig. 2b)[12]. Conversely, Tyr116 forms a hydrophobic core with the side chains of DNA-recognition loops (Fig. 2a). The Y116C mutation has low free energy change (<1 kcal $mol^{-1}$) (Fig. 2b), and is unlikely to significantly affect folding of the HMG domain, but instead may alter conformation of the DNA-recognition loop, which is important for DNA binding.

***SOX11* mutations affect downstream transcription.** Both mutations are located within the HMG domain, which is required for *SOX11* transcriptional regulation of *GDF5* (ref. 13). Luciferase assays using the *GDF5* promoter in HeLa and ATDC5 cells, showed both mutant proteins had decreased transcriptional activities compared with wild type (WT) (Fig. 3).

**SOX11 expression.** *SOX11* transcription levels were examined using multiple human complementary DNA (cDNA) panels. *SOX11* was exclusively expressed in brain (foetus and adult) and heart (adult) tissues, supporting a role for *SOX11* mutations in the brain features of CSS observed in the two patients (Supplementary Fig. 4; Supplementary Table 2).

In mice, targeted *Sox11* disruption with a β-galactosidase marker gene results in 23% birth weight reduction and lethality after the first postnatal week in homozygotes, due to hypoplastic lungs and ventricular septation defects. In addition, skeletal malformations (including phalanges) and abdominal defects are observed[14]. Physical and functional abnormalities in heterozygotes have not been described. However, in heterozygous mice, β-galactosidase expression revealed early ubiquitous expression throughout the embryo with upregulation in the central nervous system (CNS) and limb buds[14].

***sox11* knockdown experiments in zebrafish.** We further investigated *sox11* function in zebrafish. The zebrafish genome contains two orthologs of human *SOX11*, *sox11a* and *sox11b*, which are expressed in all cells until gastrulation and later become restricted to the developing CNS[15,16]. We knocked down zebrafish *sox11a* and *sox11b* (both single-exon genes) using translation-blocking morpholino oligonucleotides (MOs) (*sox11a*-MO, *sox11b*-MO and *sox11a/b*-MO), as previously described[17] (Supplementary Fig. 5a). Off-target effects of morpholino injections were excluded by repeated experiments, co-injecting with *tp53* MO or injecting into $tp53^{zdf1/zdf1}$ mutant fish[18,19]. *sox11a*- and *sox11b*-MO knockdown caused similar phenotypes, including smaller heads and body curvature (Supplementary Fig. 5b). Low-dose *sox11a*- (1.6 ng), *sox11b*- (1.6 ng) and *sox11a/b*- (1.6 ng) MO-injected embryos resulted in

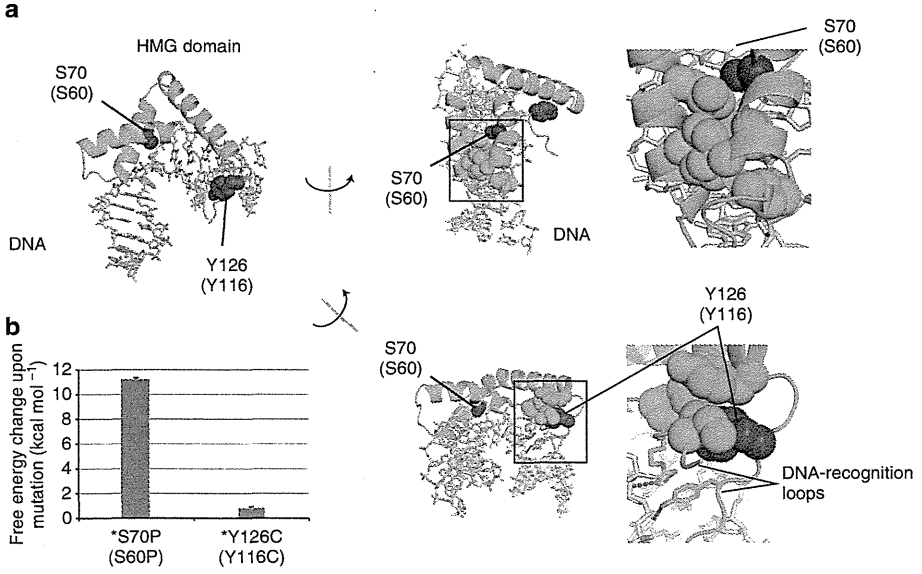


**Figure 2 | Structural effects of SOX11 mutations.** (**a**) Crystal structure of the mouse Sox4 HMG domain bound to DNA. Helices and loops are shown as green ribbons and threads, respectively. DNA is shown as grey sticks. Amino-acid residues at mutation sites are shown coloured red in the space-filling model. In the middle and right images, some of the amino-acid residues involved in the hydrophobic core surrounding mutation points are shown coloured green in the space-filling model. Amino-acid numbering is indicated for mouse Sox4 with that for human SOX11 in parentheses. Hydrogen bonds are shown as black dotted lines. Molecular structures were drawn using PyMOL (http://www.pymol.org). (**b**) Free energy changes on the indicated mutations calculated by FoldX software.

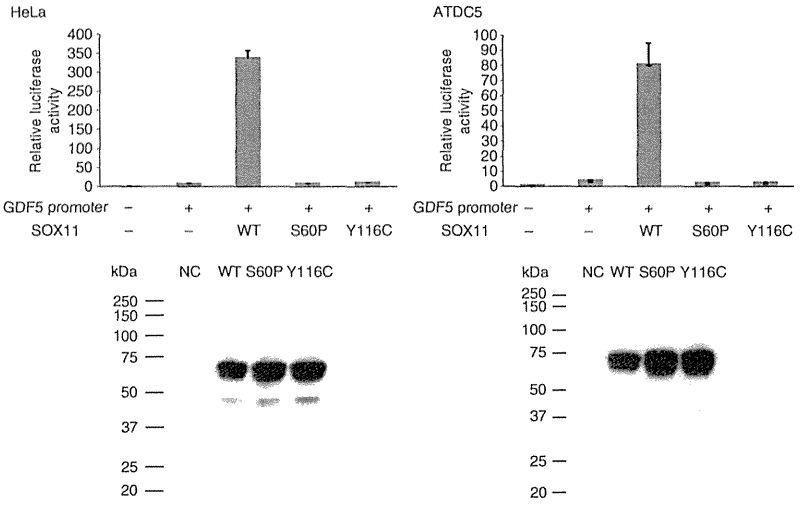


**Figure 3 | *SOX11* mutations affecting *GDF5* promoter activity.** Luciferase reporter assays measured transcriptional activity of the *GDF5* promoter (−448/+319) (UCSC genome browser hg19: chr20: 34025709-34026457) in HeLa (left) and ATDC5 (right) cells. HeLa or ATDC5 cells were co-transfected with WT or mutant (S60P and Y116C) SOX11 expression vector and reporter constructs containing either GDF5 promoter or empty vector (pGL3-basic). Relative luciferase activities compared with empty vector are presented as mean ± s.d. for two independent experiments, with each experiment performed in triplicate (upper). Immunoblot analysis of transfected HeLa and ATDC5 cell extracts showing wild-type (WT) or mutant (S60P and Y116C) SOX11 proteins (lower). Compared with WT, both SOX11 mutants reduced *GDF5* transcriptional activities in HeLa and ATDC5 cells.

significant mortality (*sox11a*-MO, ~49.3%; *sox11b*-MO, ~19.3%; *sox11a/b*-MO, ~53.0%), compared with control-MO embryos (~7.3%) (Fig. 4a). Co-injection of WT human *SOX11* mRNA (h*SOX11*-WT mRNA) with *sox11a/b*-MO improved morphant survival at 48 h post fertilization (hpf) (25.5% lethality versus 49.3% lethality with *sox11a/b*-MO alone) ($P<0.01$) (Fig. 4a; Supplementary Fig. 5c). The affected phenotype of *sox11a/b* double morphants was partially rescued by h*SOX11*-WT mRNA overexpression (4.5% normal for *sox11a/b*-MO alone versus 36.5% for co-injection with h*SOX11*-WT mRNA and *sox11a/b*-MO, $P<0.01$) (Fig. 4a). In contrast, co-injection of either mutant h*SOX11* mRNA (h*SOX11*-S60P and -Y116C mRNA) with *sox11a/b*-MO showed no significant rescue effects on lethal and affected phenotypes (Fig. 4a). There were significantly more normal phenotypes following h*SOX11*-WT mRNA and *sox11a/b*-MO co-injection, than with h*SOX11*-mutant mRNA co-injections ($P<0.05$). Head sizes in randomly selected embryos ($n\geq10$) of *sox11a* and *sox11a/b* morphants at 48 hpf were significantly decreased ($P<0.05$ in both), but not significantly changed in *sox11b* morphant. Overexpression of h*SOX11*-WT mRNA restores *sox11a/b* double-morphant head size (in randomly selected embryos, $n\geq10$), suggesting specific *sox11* suppression by morpholino injection (Fig. 4b). Although the head size of h*SOX11*-mutant mRNA and *sox11a/b*-MO-injected embryos was slightly decreased, no significant difference was recognized between overexpression of h*SOX11*-WT or h*SOX11*-mutant mRNA and *sox11a/b*-MO co-injection (Fig. 4b).Staining with acridine orange and terminal deoxynucleotidyl TdT-mediated dUTP nick end labelling (TUNEL), found significant apoptotic increases exclusively in microcephalic embryos (Fig. 4c; Supplementary Fig. 6). Brain cell death was prevented by co-injection with h*SOX11*-WT mRNA, but not by mutant h*SOX11* mRNAs (Fig. 4c). We also used HuC/D (a marker for early postmitotic and mature neurons) and acetylated tubulin (an axonal marker) immunostaining at 48 hpf to analyse neuronal cells in more detail (Supplementary Fig. 7). Decreased HuC/D-positive neurons, especially in the telencephalon and diencephalon, were observed in *sox11* morphants (Supplementary Fig. 7a). The phenotype in *sox11a/b*-MO-injected embryos was efficiently rescued by h*SOX11*-WT mRNA (Supplementary Fig. 7a). Reduction of HuC/D-positive neurons was unaltered by mutant h*SOX11* mRNA overexpression and *sox11a/b*-MO injection (Supplementary Fig. 7a). Anti-acetylated tubulin staining also showed severely reduced axonal numbers in the forebrain, midbrain and hindbrain of *sox11* morphants, compared with control-MO-injected embryos (Supplementary Fig. 7b). *sox11a/b* morphants showed phenotypic rescue when co-injected with h*SOX11*-WT mRNA, compared with mutant h*SOX11* mRNAs (Supplementary Fig. 7b).

## Discussion

We have identified *SOX11* mutations in CSS. This is the first report of human mutations in *SOXC* (*SOX4*, *SOX11* and *SOX12*)[20]. *SOX11*/*sox11* is required for neurogenesis, and loss of function in early embryos is sufficient to impair normal CNS development. Haploinsufficiency of other *SOX* genes (*SOX2*, *SOX9* and *SOX10*) is known to cause human diseases[21–23]. It is interesting that mutations of *SOX11* and other BAF subunit genes are mutually exclusive in CSS.

Sox11 was recently shown to form a transcriptional cross-regulatory network downstream of the Pax6–BAF complex. The network drives neurogenesis and converts postnatal glia into neurons[24]. Brg1 (Smarca4) binds to the *Sox11* promoter, and interaction with Pax6 is sufficient to induce Sox11 expression in neurosphere-derived cells in a Brg1-dependent manner[24]. Therefore, the Pax6–BAF complex activates a cross-regulatory transcriptional network, maintaining high expression of genes involved in neuronal differentiation and execution of cell lineage decisions[24]. *SOX11* mutations appear to be a rare cause of CSS as only 2 out of 92 patients (2.2%) showed *SOX11* abnormality and to be limited to the mild end of CSS phenotype. Abnormality of the upstream BAF complex tends to show a more severe phenotype compared with that of a downstream *SOX11* mutation, which may indicate rather specific effects of *SOX11* mutations on the CSS phenotype.

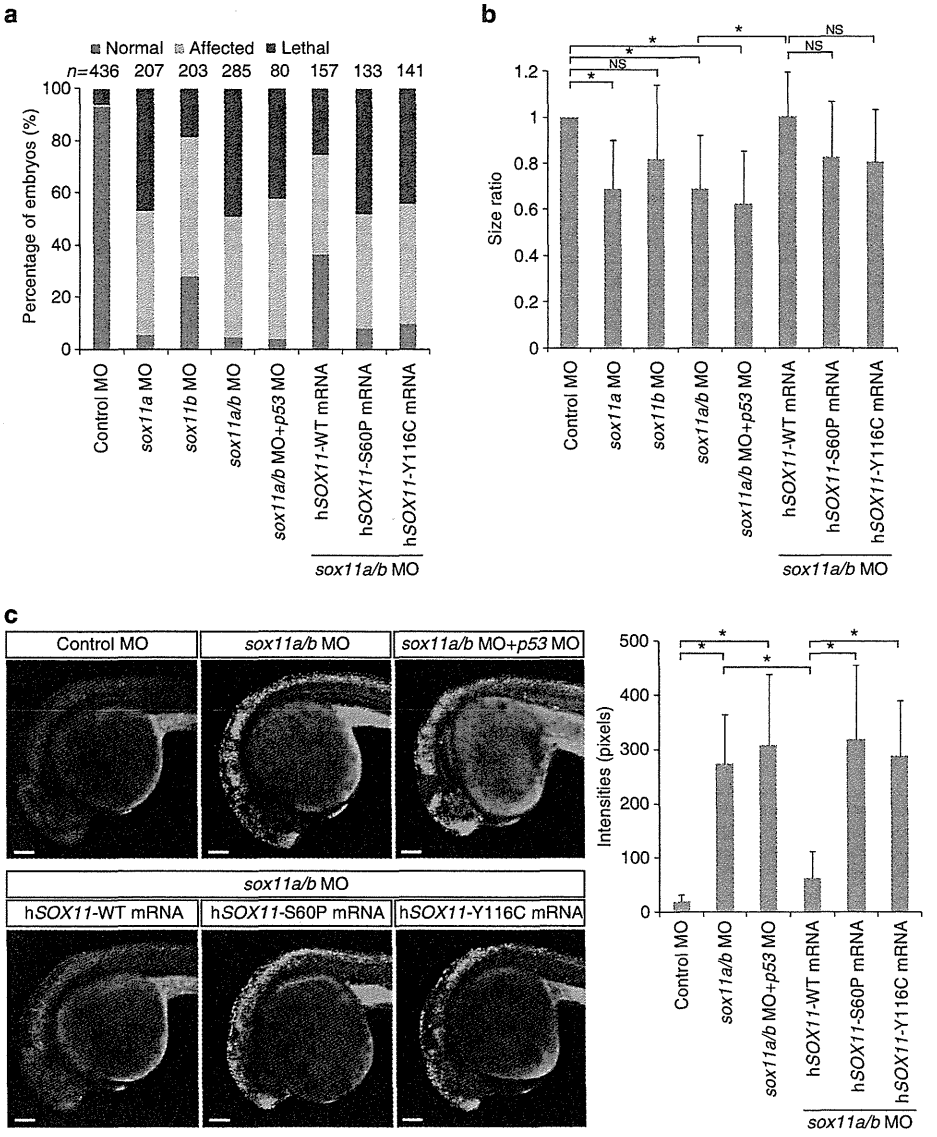


**Figure 4 | *sox11a/b* knockdown experiments in zebrafish.** (**a**) Embryos were injected with *sox11*-MO alone or with *sox11*- and *tp53*-MO or with *sox11*-MO and *in vitro* transcribed human *SOX11* (h*SOX11*) mRNA (WT, wild type; S60P, p.Ser60Pro; Y116C, p.Tyr116Cys). Injected embryos were categorized as normal, affected and lethal at 48 hpf. The lethal and affected phenotype in *sox11a/b*-MO-injected embryos was partially rescued by WT h*SOX11* mRNA overexpression. All experiments were performed more than twice and evaluated statistically with a Student's *t*-test. (**b**) Head size ratios of embryos with control-, *sox11a*-, *sox11b*- or *sox11a/b*-MO alone, or with *sox11a/b*- and *tp53*-MO or *sox11a/b*-MO and h*SOX11* mRNA (WT or mutant) at 48 hpf ($n \geq 10$) (average of control-MO as 1). Dorsal views of midbrain width were measured. Data are represented as mean ± s.d. $^*P < 0.05$ by Student's *t*-test. NS, not significant. (**c**) Brain cell death in MO-injected embryos at 30 hpf using acridine orange staining (lateral view). *sox11* morphants show increased cell death in the CNS. Scale bar, 100 μm. Quantification of acridine orange intensities in morphants are shown graphically (right, $n \geq 10$). Data are represented as mean ± s.d. $^*P < 0.001$ by Student's *t*-test.

In conclusion, mutations in both BAF complex genes and *SOX11* result in the same phenotype (CSS), providing strong support for the BAF complex and SOX11 function in a common pathway, and play an important role in human brain development.

## Methods

**Subjects and clinical data.** Patients were seen by their attending clinical geneticists. DNA samples were isolated from peripheral blood leukocytes using standard methods. Informed consent was obtained from the parents of the patients for experimental protocols and displaying participants' facial appearances in publications. This study was approved by the institutional review board of Yokohama City University School of Medicine. A total of 92 patients were analysed, including 71 patients from a previous cohort and 21 new patients.

**WES.** Trio-based WES was performed in two families. Briefly, 3 μg of genomic DNA was sheared using the Covaris 2S system (Covaris, Woburn, MA) and partitioned using SureSelect Human All Exon V4 or V4 + UTRs (Agilent Technology, Santa Clara, CA), according to the manufacturer's instructions. Exon-enriched DNA libraries were sequenced using HiSeq2000 (Illumina, San Diego, CA) with 101-bp paired-end reads and 7-bp index reads. Four samples (2.5 pM each, with different indexes) were run in one lane. Image analysis and base calling were performed using HiSeq Control Software/Real-Time Analysis and CASAVA1.8.2 (Illumina). Mapping to human genome hg19 was performed using Novoalign (http://www.novocraft.com/main/page.php?s=novoalign). Aligned reads were

processed by Picard (http://picard.sourceforge.net) to remove PCR duplicates. Variants were called using the Genome Analysis Toolkit 1.5–21 (GATK v3) with best practice variant detection (http://gatkforums.broadinstitute.org/discussion/15/best-practice-variant-detection-with-the-gatk-v1-x-retired), and annotated by Annovar (23 February 2012) (http://www.openbioinformatics.org/annovar/). Common variants registered in dbSNP137 (MAF≥0.01) (http://genome.ucsc.edu/cgi-bin/hgTrackUi?hgsid=281702941&c=chr1&g=snp137Flagged) were removed.

**Prioritization of variants.** From all the variants within exons and ±2 bp of intronic regions from exon–intron boundaries, those registered in either dbSNP137, 1,000 Genomes (http://www.1000genomes.org/), ESP 6500 (http://evs.gs.washington.edu/EVS/) or our in-house (exome data from 408 individuals) databases, and those located within segmental duplications, were removed and we focused on heterozygous non-synonymous and splice site variants, which were subsequently confirmed by Sanger sequencing. *SOX11* mutations in LOVD, http://www.LOVD.nl/SOX11.

**Structural modelling and free energy calculations.** The crystal structure of the mouse Sox4 HMG domain bound to DNA (Protein Data Bank code 3U2B) was selected by SWISS-MODEL server 5 (ref. 25) as the structure most resembling human SOX11. To examine the missense mutations, mutational free energy changes were calculated using FoldX software (version 3.0)[10,11]. Calculations were repeated three times, and resultant data presented as average values with s.d.

***SOX11* expression analysis in human tissues.** TaqMan quantitative real-time PCR was performed using cDNAs from adult (Human MTC Panel I, #636742, Clontech Laboratories, Mountain View, CA) and foetus (Human Fetal MTC Panel, #636747, Clontech Laboratories). Pre-designed TaqMan probes for human *SOX11* (Hs00167060_m1, Life Technologies Co., Carlsbad, CA) and human beta-actin (ACTB, 4326315E, Life Technologies Co.) were used. PCR was performed on a Rotor-Gene Q (QIAGEN, Valencia, CA) and expression levels normalized to *ACTB*, an internal standard gene, according to the $2^{-\Delta\Delta Ct}$ method. Kidney expression was used as the standard (1×).

**Expression vectors.** The *SOX11* open-reading frame clone was purchased from Promega (Tokyo, Japan) and *SOX11* mutants (c.178T>C; p.Ser60Pro and c.347A>G; p.Tyr116Cys) generated by site-directed mutagenesis with the KOD-Plus-Mutagenesis Kit (TOYOBO, Osaka, Japan). WT and mutant *SOX11* cDNAs were PCR amplified and cloned into the pEF6/V5-His B mammalian expression vector (Life Technologies) using the In-Fusion PCR Cloning Kit (Clontech Laboratories), and also into the p3xFLAG-CMV-14 mammalian expression vector (Sigma, St Louis, MO). The *GDF5* promoter 5′-flanking sequence (−448/+319) was PCR amplified and cloned into the pGL3-basic vector (Promega). All constructs were verified by Sanger sequencing. Human *SOX11* cDNA can be obtained from GenBank/EMBL/DDBJ nucleotide core database under the accession code AB028641.1.

**Immunostaining.** Mouse neuroblastoma 2A (Neuro-2A) cells were cultured in Dulbecco's modified Eagle's medium (DMEM)–high glucose GlutaMAX supplemented with 10% fetal bovine serum (FBS) and penicillin-streptomycin (Life Technologies Co.). Neuro-2A cells were plated into 24-well plates, 24 h before transfection. Each expression construct (200 ng) was transfected into Neuro-2A cells using X-tremeGENE 9 DNA Transfection Reagent (Roche Diagnostics, Indianapolis, IN). Twenty-four hours after transfection, cells were fixed in 4% paraformaldehyde (PFA)/phosphate-buffered saline (PBS) for 15 min at room temperature, and permeabilized in 0.1% Triton X-100/PBS for 5 min at room temperature. C-terminal V5-6xHis-tagged SOX11 proteins were detected using a mouse anti-V5 primary antibody (1:200; Life Technologies Co.) and an Alexa Fluor 546 Goat Anti-Mouse IgG secondary antibody (1:1,000; Life Technologies Co.). Smears were mounted in Vectashield mounting medium with DAPI (Vector Lab., Burlingame, CA). Confocal images were acquired using a Fluoview FV1000-D microscope (Olympus, Tokyo, Japan).

**Luciferase assay.** HeLa cells were cultured in DMEM-high glucose supplemented with penicillin (50 units ml$^{-1}$), streptomycin (50 μg ml$^{-1}$) and 10% FBS. ATDC5 cells were cultured in DMEM/Ham's F-12 (1:1) supplemented with the above antibiotics and 5% FBS. Cells were plated in 24-well plates, 24 h before transfection, and transfections performed using TransIT-LT1 (Takara, Ohtsu, Japan) with pGL3 reporter (500 ng per well), effector (250 ng per well) and pRL-SV40 internal control (6 ng per well) vectors. Twenty-four hours after transfection, cells were harvested and luciferase activities measured using the PicaGene Dual SeaPansy Luminescence Kit (TOYO B-Net, Tokyo, Japan). Production of WT and mutant SOX11 proteins was assessed by immunoblot analysis with monoclonal anti-FLAG M2 HRP antibody (1:3,000; Sigma), following the manufacturer's instructions.

**Morpholino and mRNA microinjection.** Antisense translation-blocking morpholinos (MOs) for *sox11a*—(5′-CGCTGTTGTCCGTTTGCTGCACCAT-3′), *sox11b*—(5′-CTGTGCTCCGTCTGCTGCACCATGT-3′)[17], *tp53*—(5′-GCGCCATTGCTTTGCAAGAATTG-3′)[18] and standard control—(5′-CCTCTTACCTCAGTTACAATTTATA-3′) MO were obtained from GeneTools (Philomath, OR) and injected (or co-injected) into one- to two-cell-stage embryos at a final concentration of 0.1 or 0.2 mM. In rescue assays, capped human *SOX11* mRNAs transcribed *in vitro* from pEF6/V5-His B constructs were prepared using the mMessage mMachine T7 ULTRA Transcription Kit (Ambion, Carlsbad, CA), following the manufacturer's instructions, and injected into one-cell-stage embryos. For each MO knockdown and rescue experiment, embryos from the same clutch were used as experimental subjects and controls. Approximately 1 μg of capped RNA was injected per embryo. The experiment was authorized by the institutional committee of fish experiments in the National Research Institute of Fisheries Science.

**Cell death detection.** To detect apoptotic cells in live embryos, embryos at 30 hpf were manually dechorionated and incubated in acridine orange (2 μg ml$^{-1}$ in egg water) at 28 °C for 1 h. After washing with egg water six times for 10 min each, embryos were anaesthetized with tricaine, mounted in 2% methylcellulose and examined by confocal microscopy. Apoptotic cells were also examined by the TUNEL assay, as previously described[26]. Embryos at 30 hpf, were fixed overnight in 4% PFA with PBS at 4 °C and stored in 100% methanol at −20 °C. Samples were incubated in 100% acetone at −20 °C for 20 min. Following fixation, the embryos were rinsed three times with PBS containing 0.1% Tween-20. Samples were then permeabilized by treatment with 0.5% Triton X-100 and 0.1% sodium citrate in PBS for 15 min. Embryos were subjected to the TUNEL assay by using the ApopTag Red *in situ* Apoptosis Detection Kit (Merck KGaA Millipore, Darmstadt, Germany) according to the manufacture's instruction.

**Detection and quantitation of visible and fluorescent images.** All animals were photographed under the same conditions using a LSM510 confocal microscope (Carl Zeiss, Jena, Germany). In each animal, acridine orange-positive cells were quantitated using a selection tool in Adobe Photoshop, for a colour range chosen by green colour selection of regions showing visually positive acridine orange staining. For analysis of embryos, defined head regions were selected in each embryo. Following pixel selection, a fuzziness setting of 0 was used, and chosen pixel numbers calculated using the image histogram calculation.

**Whole-mount immunohistochemistry.** For HuC/D staining, embryos at 48 hpf were fixed in 4% PFA overnight at 4 °C and dehydrated in methanol at −20 °C. For acetylated tubulin staining, embryos at 48 hpf were fixed in Dent's fixative (80% methanol and 20% dimethyl sulphoxide) overnight at 4 °C. Embryos were permeabilized with proteinase K followed by postfixation with 4% PFA and washed with PBSTX (PBS containing 0.5% Triton X-100). After treating with 4% normal goat serum (NGS) in PBSTX for 2 h at room temperature, embryos were incubated with mouse anti-HuC/D (1:500, A21271, Life Technologies Co.) or mouse anti-acetylated tubulin (1:1,000, T7451, Sigma) antibodies in 4% NGS/PBSTX overnight at 4 °C. Embryos were washed five times with PBSTX for 10 min each and incubated with goat anti-mouse fluorescein isothiocyanate secondary antibody diluted in 2% NGS/PBSTX for 2 h at room temperature. After washing five times for 10 min each, embryos were mounted in 2% methylcellulose and examined using a Fluoview FV1000-D confocal microscope (Olympus).

## References


1. Ronan, J. L., Wu, W. & Crabtree, G. R. From neural development to cognition: unexpected roles for chromatin. *Nat. Rev. Genet.* **14,** 347–359 (2013).
2. Tsurusaki, Y. *et al.* Mutations affecting components of the SWI/SNF complex cause Coffin-Siris syndrome. *Nat. Genet.* **44,** 376–378 (2012).
3. Tsurusaki, Y. *et al.* Coffin-Siris syndrome is a SWI/SNF complex disorder. *Clin. Genet.* **85,** 548–554 (2014).
4. Santen, G. W. E. *et al.* Mutations in SWI/SNF chromatin remodeling complex gene ARID1B cause Coffin-Siris syndrome. *Nat. Genet.* **44,** 379–380 (2012).
5. Santen, G. W. E. *et al.* Coffin-Siris syndrome and the BAF complex: genotype-phenotype study in 63 patients. *Hum. Mutat.* **34,** 1519–1528 (2013).
6. Wieczorek, D. *et al.* A comprehensive molecular study on Coffin-Siris and Nicolaides-Baraitser syndromes identifies a broad molecular and clinical spectrum converging on altered chromatin remodeling. *Hum. Mol. Genet.* **22,** 5121–5135 (2013).
7. Van Houdt, J. K. *et al.* Heterozygous missense mutations in SMARCA2 cause Nicolaides-Baraitser syndrome. *Nat. Genet.* **44,** 445–449 (2012).
8. Kosho, T. *et al.* Clinical correlations of mutations affecting six components of the SWI/SNF complex: detailed description of 21 patients and a review of the literature. *Am. J. Med. Genet. A* **161,** 1221–1237 (2013).
9. Jauch, R., Ng, C. K., Narasimhan, K. & Kolatkar, P. R. The crystal structure of the Sox4 HMG domain-DNA complex suggests a mechanism for positional interdependence in DNA recognition. *Biochem. J.* **443,** 39–47 (2012).
10. Guerois, R., Nielsen, J. E. & Serrano, L. Predicting changes in the stability of proteins and protein complexes: a study of more than 1000 mutations. *J. Mol. Biol.* **320,** 369–387 (2002).

11. Schymkowitz, J. *et al.* The FoldX web server: an online force field. *Nucleic Acids Res.* **33,** W382–W388 (2005).
12. Khan, S. & Vihinen, M. Performance of protein stability predictors. *Hum. Mutat.* **31,** 675–684 (2010).
13. Kan, A. *et al.* SOX11 contributes to the regulation of GDF5 in joint maintenance. *BMC Dev. Biol.* **13,** 4 (2013).
14. Sock, E. *et al.* Gene targeting reveals a widespread role for the high-mobility-group transcription factor Sox11 in tissue remodeling. *Mol. Cell. Biol.* **24,** 6635–6644 (2004).
15. Rimini, R. *et al.* Expression patterns of zebrafish sox11A, sox11B and sox21. *Mech. Dev.* **89,** 167–171 (1999).
16. de Martino, S. *et al.* Expression of sox11 gene duplicates in zebrafish suggests the reciprocal loss of ancestral gene expression patterns in development. *Dev. Dyn.* **217,** 279–292 (2000).
17. Gadi, J. *et al.* The transcription factor protein sox11 enhances early osteoblast differentiation by facilitating proliferation and the survival of mesenchymal and osteoblast progenitors. *J. Biol. Chem.* **288,** 25400–25413 (2013).
18. Robu, M. E. *et al.* p53 activation by knockdown technologies. *PLoS Genet.* **3,** e78 (2007).
19. Berghmans, S. *et al.* tp53 mutant zebrafish develop malignant peripheral nerve sheath tumors. *Proc. Natl Acad. Sci. USA* **102,** 407–412 (2005).
20. Sarkar, A. & Hochedlinger, K. The sox family of transcription factors: versatile regulators of stem and progenitor cell fate. *Cell Stem Cell* **12,** 15–30 (2013).
21. Fantes, J. *et al.* Mutations in SOX2 cause anophthalmia. *Nat. Genet.* **33,** 461–463 (2003).
22. Pingault, V. *et al.* SOX10 mutations in patients with Waardenburg-Hirschsprung disease. *Nat. Genet.* **18,** 171–173 (1998).
23. Wagner, T. *et al.* Autosomal sex reversal and campomelic dysplasia are caused by mutations in and around the SRY-related gene SOX9. *Cell* **79,** 1111–1120 (1994).
24. Ninkovic, J. *et al.* The BAF complex interacts with Pax6 in adult neural progenitors to establish a neurogenic cross-regulatory transcriptional network. *Cell Stem Cell* **13,** 403–418 (2013).
25. Kiefer, F., Arnold, K., Kunzli, M., Bordoli, L. & Schwede, T. The SWISS-MODEL Repository and associated resources. *Nucleic Acids Res.* **37,** D387–D392 (2009).
26. Koshimizu, E. *et al.* Embryonic senescence and laminopathies in a progeroid zebrafish model. *PLoS ONE* **6,** e17688 (2011).


## Acknowledgements

We thank the individuals and their families for participation in this study. We also thank Nobuko Watanabe for her technical assistance. This work was supported by the Ministry of Health, Labour and Welfare of Japan; the Japan Society for the Promotion of Science (a Grant-in-Aid for Scientific Research (B), and a Grant-in-Aid for Scientific Research (A)); the Takeda Science Foundation; the fund for Creation of Innovation Centers for Advanced Interdisciplinary Research Areas Program in the Project for Developing Innovation Systems; the Strategic Research Program for Brain Sciences; and a Grant-in-Aid for Scientific Research on Innovative Areas (Transcription Cycle) from the Ministry of Education, Culture, Sports, Science and Technology of Japan. The Indian Council of Medical Research, New Delhi is also appreciated for funding support for the DNA banking facility.

## Author contributions

Y.T. and N.Ma. designed and directed the study. Y.T., E.K. and N.Ma. wrote the manuscript. H.O. and S.P. collected samples and provided subjects' clinical information. N.O. evaluated clinical information. Y.T., T.S., S.M., M.N., H.S., S.W., K.-i.Y. and N.Mi. performed exome and Sanger sequencing. E.K., S.Ima. and M.Y. performed zebrafish experiments. I.K. and S.Ike. performed luciferase assays. M.S. and K.O. performed crystal structural analysis. Y.T. and H.K. analysed protein localization.

## Additional information

**Accession codes:** Exome sequence data for CSS patients have been deposited in the Human Genetic Variation Browser under the accession code HGV0000001 (http://www.genome.med.kyoto-u.ac.jp/SnpDB/repository/HGV0000001.html). Access to this data is controlled by the Yokohama City University Data Access Committee.

**Supplementary Information** accompanies this paper at http://www.nature.com/naturecommunications

**Competing financial interests:** The authors declare no competing financial interests.

**Reprints and permission** information is available online at http://npg.nature.com/reprintsandpermissions/

**How to cite this article:** Tsurusaki, Y. *et al. De novo SOX11* mutations cause Coffin–Siris syndrome. *Nat. Commun.* 5:4011 doi: 10.1038/ncomms5011 (2014).

# Expanding the phenotypic spectrum of *TUBB4A*-associated hypomyelinating leukoencephalopathies

Satoko Miyatake, MD, PhD
Hitoshi Osaka, MD, PhD
Masaaki Shiina, MD, PhD
Masayuki Sasaki, MD, PhD
Jun-ichi Takanashi, MD, PhD
Kazuhiro Haginoya, MD, PhD
Takahito Wada, MD, PhD
Masafumi Morimoto, MD, PhD
Naoki Ando, MD, PhD
Yoji Ikuta, MD
Mitsuko Nakashima, MD, PhD
Yoshinori Tsurusaki, PhD
Noriko Miyake, MD, PhD
Kazuhiro Ogata, MD, PhD
Naomichi Matsumoto, MD, PhD
Hirotomo Saitsu, MD, PhD

Correspondence to Dr. Matsumoto: naomat@yokohama-cu.ac.jp or Dr. Saitsu: hsaitsu@yokohama-cu.ac.jp

## ABSTRACT

**Objective:** We performed whole-exome sequencing analysis of patients with genetically unsolved hypomyelinating leukoencephalopathies, identifying 8 patients with *TUBB4A* mutations and allowing the phenotypic spectrum of *TUBB4A* mutations to be investigated.

**Methods:** Fourteen patients with hypomyelinating leukoencephalopathies, 7 clinically diagnosed with hypomyelination with atrophy of the basal ganglia and cerebellum (H-ABC), and 7 with unclassified hypomyelinating leukoencephalopathy, were analyzed by whole-exome sequencing. The effect of the mutations on microtubule assembly was examined by mapping altered amino acids onto 3-dimensional models of the αβ-tubulin heterodimer.

**Results:** Six heterozygous missense mutations in *TUBB4A*, 5 of which are novel, were identified in 8 patients (6/7 patients with H-ABC [the remaining patient is an atypical case] and 2/7 patients with unclassified hypomyelinating leukoencephalopathy). In 4 cases with parental samples available, the mutations occurred de novo. Analysis of 3-dimensional models revealed that the p.Glu410Lys mutation, identified in patients with unclassified hypomyelinating leukoencephalopathy, directly impairs motor protein and/or microtubule-associated protein interactions with microtubules, whereas the other mutations affect longitudinal interactions for maintaining αβ-tubulin structure, suggesting different mechanisms in tubulin function impairment. In patients with the p.Glu410Lys mutation, basal ganglia atrophy was unobserved or minimal although extrapyramidal features were detected, suggesting its functional impairment.

**Conclusions:** *TUBB4A* mutations cause typical H-ABC. Furthermore, *TUBB4A* mutations associate cases of unclassified hypomyelinating leukoencephalopathies with morphologically retained but functionally impaired basal ganglia, suggesting that *TUBB4A*-related hypomyelinating leukoencephalopathies encompass a broader clinical spectrum than previously expected. Extrapyramidal findings may be a key for consideration of *TUBB4A* mutations in hypomyelinating leukoencephalopathies. ***Neurology*® 2014;82:2230–2237**

## GLOSSARY

**4H** = hypomyelination, hypodontia, and hypogonadotropic hypogonadism; **H-ABC** = hypomyelination with atrophy of the basal ganglia and cerebellum; **MAP** = microtubule-associated protein; **MREI** = Met-Arg-Glu-Ile; ***TUBB4A*** = tubulin, beta 4A class IVa.

Leukoencephalopathies are a heterogeneous group of disorders affecting the white matter of the brain. It is estimated that approximately 30% to 40% of patients with leukoencephalopathy remain without a specific diagnosis despite extensive investigations.[1] Brain MRI aids diagnosis because distinct MRI patterns enable easier detection of white matter abnormalities and successful categorization.[1,2] Moreover, recent advances in whole-exome sequencing have improved understanding of these clinically defined/undefined disease entities by identifying genetic causes and their phenotypic spectrum. For example, the majority of cases with hypomyelination,

**Supplemental data at Neurology.org**

From the Departments of Human Genetics (S.M., M.N., Y.T., N. Miyake, N. Matsumoto, H.S.) and Biochemistry (M. Shiina, K.O.), Yokohama City University Graduate School of Medicine; Division of Neurology (H.O.), Clinical Research Institute, Kanagawa Children's Medical Center, Yokohama; Department of Pediatrics (H.O.), Jichi Medical School, Tochigi; Department of Child Neurology (M. Sasaki), National Center of Neurology and Psychiatry, Tokyo; Department of Pediatrics (J.-i.T.), Kameda Medical Center, Chiba; Department of Pediatric Neurology (K.H.), Takuto Rehabilitation Center for Children, Sendai; Genetic Counselling and Clinical Research Unit (T.W.), Kyoto University School of Public Health; Department of Pediatrics (M.M.), Graduate School of Medical Science, Kyoto Prefectural University of Medicine; Department of Neonatology and Pediatrics (N.A.), Nagoya City University Graduate School of Medical Sciences; and Department of Neurology (Y.I.), Tokyo Metropolitan Children's Medical Center, Japan.

Go to Neurology.org for full disclosures. Funding information and disclosures deemed relevant by the authors, if any, are provided at the end of the article.

hypodontia, and hypogonadotropic hypogonadism (4H syndrome),[3–5] tremor-ataxia with central hypomyelination leukodystrophy (TACH),[6] leukodystrophy with oligodontia (LO),[7,8] or hypomyelination with cerebellar atrophy and hypoplasia of the corpus callosum (HCAHC),[9] which was described in Japan, share some clinical overlap and have *POLR3A* or *POLR3B* mutations in common.[10–14]

Hypomyelination with atrophy of the basal ganglia and cerebellum (H-ABC)[15,16] is characterized by early-onset motor regression and/or delay followed by extrapyramidal symptoms, distinguishing H-ABC from other hypomyelinating leukoencephalopathies caused by *POLR3A* or *POLR3B* mutations. A recurrent de novo *TUBB4A* mutation was recently reported in 11 patients with H-ABC.[17] Of note, *TUBB4A* mutations also cause autosomal dominant DYT4 dystonia,[18,19] a condition that presents with normal brain MRI findings. This suggests that in addition to H-ABC, *TUBB4A* mutations may be widely related to other hypomyelinating leukoencephalopathies. Herein, we describe 8 patients with *TUBB4A* mutations identified by whole-exome sequencing, clarifying their phenotypic spectrum.

**METHODS Study subjects.** Fourteen patients with molecularly undiagnosed hypomyelinating leukoencephalopathy were included in the study. Patients were diagnosed based on clinical symptoms and brain MRI findings. Among the 14 patients, 7 were clinically diagnosed with H-ABC and 7 with hypomyelinating leukoencephalopathy that did not meet the criteria for H-ABC, 4H syndrome, or Pelizaeus-Merzbacher disease. Patients with *POLR3A* or *POLR3B* mutations were excluded from this cohort. When available, parental samples were also tested in mutation-positive patients.

**Standard protocol approvals, registrations, and patient consents.** Experimental protocols were approved by the Committee for Ethical Issues at Yokohama City University School of Medicine. Written informed consent was obtained from all patients or their parents.

**Mutation analysis.** We performed whole-exome sequencing in 14 patients. Genomic DNA was captured using the SureSelect$^{XT}$ Human All Exon 50 Mb (v3) or 51 Mb (v4) Kit (Agilent Technologies, Santa Clara, CA) and sequenced on either the GAIIx platform (Illumina, San Diego, CA) with 108–base pair paired-end reads or HiSeq2000 (Illumina) with 101–base pair paired-end reads. After filtering against dbSNP135 and 91 in-house normal control exomes, rare protein-altering and splice-site variant calls were obtained for each patient. We identified *TUBB4A* mutation calls and confirmed these mutations by Sanger sequencing. In 4 of 8 patients with *TUBB4A* mutations, parental samples were analyzed by Sanger sequencing to determine the mode of inheritance.

**Three-dimensional structure modeling.** To determine the effect of *TUBB4A* mutations on microtubule assembly, we mapped mutation positions onto the 3-dimensional structure of the αβ-tubulin heterodimer (Protein Data Bank code 1JFF)[20] and examined their interaction with surrounding molecules.

**RESULTS Identification of *TUBB4A* mutations.** Whole-exome sequencing identified 6 heterozygous missense mutations in *TUBB4A*, in 6 of 7 patients with H-ABC (85.7%) and 2 of 7 patients with unclassified hypomyelinating leukoencephalopathy (28.6%) (see table 1 and tables e-1 and e-2 on the *Neurology*® Web site at Neurology.org). Two mutations, c.1228G>A (p.Glu410Lys) and c.745G>A (p.Asp249Asn), were identified in 2 unrelated patients. Two hypomyelinating patients with similar clinical features as those previously reported,[9] carried the c.1228G>A mutation. The c.745G>A mutation was a recurrent mutation reported in patients with H-ABC.[17] The other 5 mutations were novel. None of the mutations were registered in the National Heart, Lung, and Blood Institute Exome Sequencing Project (ESP6500), 1000 Genomes, or our 575 in-house control exomes. The c.5G>A (p.Arg2Gln) missense mutation, identified in a patient with H-ABC, alters Arg2 to Gln. Arg2 is located within the highly conserved, amino-terminal β-tubulin tetrapeptide Met-Arg-Glu-Ile (MREI) motif and is involved in autoregulatory mechanisms for β-tubulin stability. Notably, Arg2 is altered to Gly in a large family with DYT4.[18,19] All of the mutations occur within highly conserved residues, from yeast to human, and among human β-tubulins (figure 1). GERP (Genomic Evolutionary Rate Profiling) scores were high for all mutated residues, and Web-based prediction programs identified all mutations as pathogenic (table e-1). In 4 patients with parental samples available, the mutations occurred de novo (table e-1). In 2 patients, only the mother's sample was available and confirmed as mutation-negative.

**Three-dimensional structural modeling analysis.** Tubulin heterodimers polymerize longitudinally in a head-to-tail manner, forming protofilaments, which then laterally interact with each other to form microtubules (figure 2). Some mutations fall within longitudinal interaction interfaces, whereas others are near interaction regions for motor proteins and microtubule-associated proteins (MAPs).[21,22] Thr178 of β-tubulin is located at a longitudinal interheterodimer interface, in proximity to the guanine nucleotide–binding pocket of β-tubulin (figure 2). This residue is reportedly important for regulation of αβ-tubulin heterodimer polymerization with GTP[23,24]; therefore, the Thr178Arg mutation may affect the polymerization process. Arg2 and Asp249 of β-tubulin are

**Table 1** Clinical features of the patients

| | Patient 1[9] | Patient 2[9] | Patient 3 | Patient 4[26] | Patient 5[27] | Patient 6 | Patient 7 | Patient 8 |
|---|---|---|---|---|---|---|---|---|
| **Current age, y, sex** | 23, M | 41, M | 15, F | 12, M | 16, M | 10, M | 4, M | 1, F |
| **Mutation** | c.1228G>A | c.1228G>A | c.5G>A | c.745G>A | c.1162A>G | c.745G>A | c.533C>G | c.785G>A |
| **Protein alteration** | p.Glu410Lys | p.Glu410Lys | p.Arg2Gln | p.Asp249Asn | p.Met388Val | p.Asp249Asn | p.Thr178Arg | p.Arg262His |
| **Initial diagnosis** | Unclassified hypomyelinating leukoencephalopathy[a] | Unclassified hypomyelinating leukoencephalopathy[a] | H-ABC | H-ABC | H-ABC | H-ABC | H-ABC | H-ABC |
| **Age at onset, mo** | 12 | 12 | 1.5 | 18 | 3 | 19 | 6 | 2 |
| **Maximum motor milestone** | Unsupported unstable walking | Unsupported unstable walking | No head control | Walking for a few steps | Rolling over | Supported walking | No head control | No head control |
| **Onset of motor deterioration** | 10 y | 20 y | ND | 18 mo | 3 mo | 19 mo | ND | ND |
| **Intellectual disability** | Mild | Moderate | Severe | Severe | Severe | Severe | Severe | Moderate |
| **Motor signs** | | | | | | | | |
| **Ataxia** | + | + | ND | + | ND | + | ND | ND |
| **Tremor** | + | + | − | − | − | + | − | ND |
| **Spasticity** | + | + | + | + | + | + | ND | + |
| **Babinski sign** | + | + | − | + | ND | + | − | + |
| **Rigidity** | + | + | + | + | + | + | + | − |
| **Choreoathetosis** | − | − | + | + | + | − | − | − |
| **Dystonia** | + | + | + | + | + | + | − | − |
| **Brain MRI findings** | | | | | | | | |
| **Hypomyelination** | + | + | + | + | + | + | + | + |
| **Atrophy of the basal ganglia** | − | ± | + | + | + | + | + | + |
| **Atrophy of the cerebellum** | + | + | + | + | + | + | + | − |
| **Atrophy of the corpus callosum** | + | + | + | + | + | + | + | − |

Abbreviations: H-ABC = hypomyelination with atrophy of the basal ganglia and cerebellum; ND = not determined.
Symbols: + = present; − = absent; ± = minimally detected.
[a] Unclassified hypomyelinating leukoencephalopathy: did not meet the criteria for H-ABC, 4H syndrome (hypomyelination, hypodontia, and hypogonadotropic hypogonadism), or Pelizaeus-Merzbacher disease.

located at an intraheterodimer interface (figures 2 and e-1A). These residues stabilize the β-tubulin T7 loop region, which interacts with α-tubulin within a heterodimer (figure e-1A), indicating that the p.Arg2Gln and p.Asp249Asn mutations may affect tubulin heterodimerization. Glu410 is located on the exposed outer surface that mediates interactions with motor proteins and/or MAPs (figures 2 and e-1B).[21,22] This residue is crucial for the kinesin-microtubule interaction, and thus the p.Glu410Lys mutation may directly impair motor protein and/or MAP interactions with microtubules. Arg262 and Met388 are located near the intra- and interheterodimer interfaces, respectively, and both are also near the interaction region for motor proteins and/or MAPs (figures 2 and e-1, B and C). Arg262 is involved in the hydrophobic core with residues from a loop that interacts with the α-tubulin subunit within the heterodimer, and from helix H12, which interacts with motor proteins and/or MAPs (figures 2 and e-1B). Met388 is involved in the hydrophobic core with residues from helix H11, which interacts with the α-tubulin subunit in the neighboring heterodimer, and from helix H12 (figures 2 and e-1C).[25] Thus, the p.Arg262His and the p.Met388Val mutations may destabilize the hydrophobic core and potentially affect the tertiary structure, resulting in impairment of longitudinal intra- and interheterodimer tubulin interactions, respectively, and/or interaction with motor proteins and/or MAPs.

**Clinical features.** Clinical information on patients with *TUBB4A* mutations is presented in tables 1 and e-2, and brain MRIs are shown in figures 3 and e-2.

The mean age at onset was 9.2 months, although the age at onset was varied. Initial motor development also varied, with some acquiring unsupported but

Figure 1 *TUBB4A* mutations in patients with hypomyelinating leukoencephalopathy

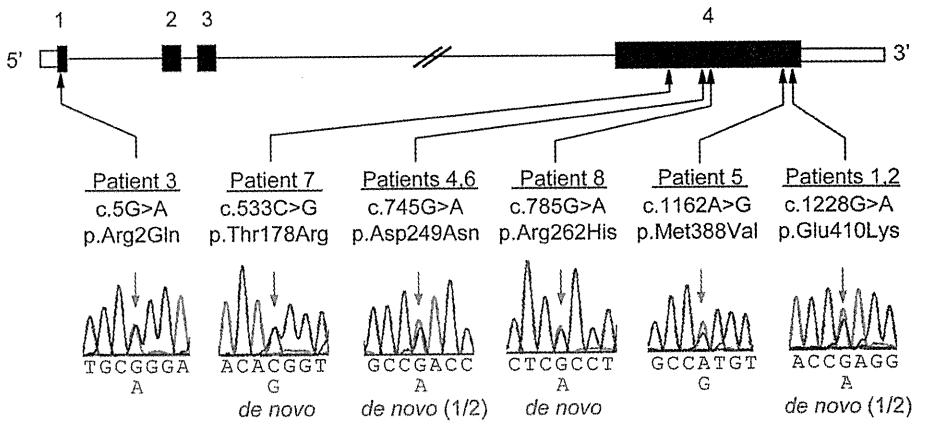


| Amino acid change | Q | R | N | H | V | K |
|---|---|---|---|---|---|---|
| H. sapiens_TUBB4A | MREIVHL | VSDTVVE | LNADLRK | PFPRLHF | FTAMFRR | EFTEAES |
| M. musculus_TUBB4A | MREIVHL | VSDTVVE | LNADLRK | PFPRLHF | FTAMFRR | EFTEAES |
| B. Taurus_TUBB4A | MREIVHL | VSDTVVE | LNADLRK | PFPRLHF | FTAMFRR | EFTEAES |
| X. tropicalis_TUBB4A | MREIVHL | VSDTVVE | LNADLRK | PFPRLHF | FTAMFRR | EFTEAES |
| D. rerio_TUBB2C | MREIVHL | VSDTVVE | LNADLRK | PFPRLHF | FTAMFRR | EFTEAES |
| TUBB4B_Human | MREIVHL | VSDTVVE | LNADLRK | PFPRLHF | FTAMFRR | EFTEAES |
| TUBB2B_Human | MREIVHI | VSDTVVE | LNADLRK | PFPRLHF | FTAMFRR | EFTEAES |
| TBB1_Human | MREIVHI | VSDTVVE | LNADLRK | PFPRLHF | FSAMFRR | EFGEAES |
| TBB_YEAST | MREIVHI | TSDTVVE | LNADLRK | PFPRLHF | FSAMFRR | EFSEAES |

*TUBB4A* schematic with the 6 mutations is presented. Untranslated regions and coding regions are shown in white and black rectangles, respectively. All mutations occur at evolutionarily conserved amino acids. Homologous sequences were aligned using CLUSTALW (http://www.genome.jp/tools/clustalw/).

unsteady walking and others never acquiring head control. The maximum motor milestone of these patients was unstable short walking. The clinical course appeared milder in patients with an older age at onset. This tendency was most prominent in patients initially diagnosed with unclassified hypomyelinating leukoencephalopathy. For example, the onset of motor deterioration started in the first or second decades in these patients but was between 0 and 3 years old in patients with typical H-ABC. Intellectual disability was mild to moderate in the former but mostly severe in the latter patients.

All clinically evaluated patients with *TUBB4A* mutations demonstrated cerebellar ataxia and spasticity. Except for patient 8, all demonstrated extrapyramidal features such as rigidity, dystonia, or choreoathetosis. In patient 1, dystonia was prominent compared with other hypomyelination patients with either *POLR3A* or *POLR3B* mutations.[9,11] Patient 8 was 1 year old at the time of the study, and brain MRI showed a relatively small but still well-retained putamen compared with healthy subjects of the same age, suggesting that extrapyramidal features may not yet have developed but would likely express as the basal ganglia atrophy progressed. Notably, both hypomyelinating patients with either very mild basal ganglia atrophy (patient 2) or none identifiable (patient 1) demonstrated extrapyramidal signs, suggesting that the basal ganglia may be impaired functionally in these patients as well as other patients with typical H-ABC. Case reports are available in appendix e-1. Patients 1 and 2,[9] 4,[26] and 5[27] were previously described. Retrospectively, patient 2 might be diagnosed with atypical H-ABC because minimal basal ganglia atrophy cannot be excluded. In the patient with H-ABC with no *TUBB4A* mutation, the atrophy of basal ganglia was very mild compared with that of patients with typical H-ABC. However, clinical symptoms are very severe with neither head control nor sitting at 12 years, suggesting that the patient has atypical H-ABC.

**DISCUSSION** The β- and α-tubulins are major components of microtubules. Microtubules have essential roles in many cellular processes including mitosis, intracellular transport, asymmetric neuronal morphology, and ciliary and flagellar motility.[28] Multiple β-tubulin isotypes are present, with high homology (differing primarily at 15–20 amino acids within the C terminus), and expressed differentially in a tissue-dependent manner.[29] Certain isotypes, namely, β-tubulin isotypes 2A, 2B, 3, and 4A, are neuron-specific proteins and highly expressed in brain.[28] In the nervous system, microtubules provide structure, generate force necessary for neuronal migration, and serve as scaffolds for motor proteins and/or MAPs to transport cargo.[30] In addition to *TUBB4A*-associated leukoencephalopathies[17] and dystonia,[18,19] *TUBA1A*, *TUBB2B*, and *TUBB3*

**Figure 2** Structural prediction of *TUBB4A* mutations in the αβ-tubulin heterodimer

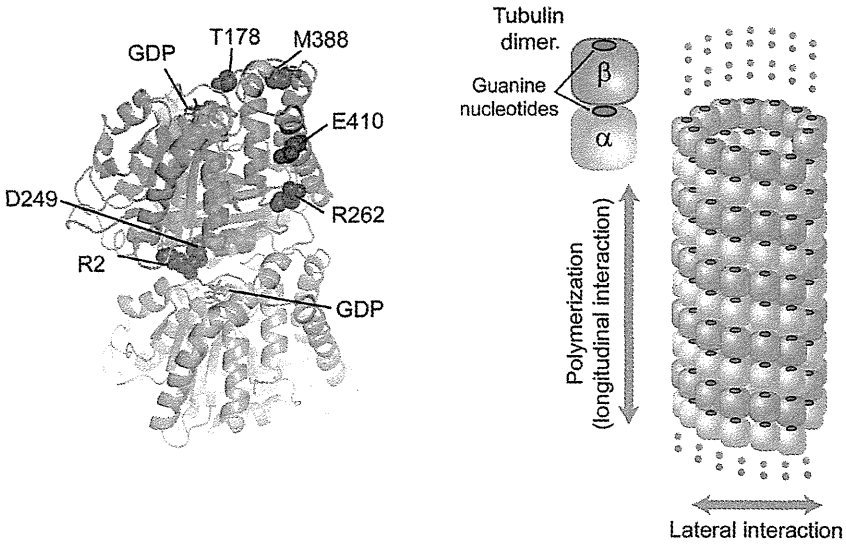


Mapping of disease-causing amino acid mutations on the αβ-tubulin heterodimer (Protein Data Bank code 1JFF) crystal structure, with schematic representation of a tubulin dimer (left) and microtubule segment (right). The α- and β-tubulins are colored gray and green, respectively. Left: The longitudinal interheterodimer interface of β-tubulin (which interacts with α-tubulin in a neighboring αβ heterodimer) is colored pink,[24] and the β-tubulin microtubule-associated protein and motor protein interaction region is colored cyan.[21,22] Side chains of residues altered by the mutations are shown in space-filling representation in red. Helices, β-sheets, and loops are shown as ribbons, arrows, and threads, respectively, and nucleotides are blue sticks. Right: Tubulin heterodimers polymerize longitudinally to form protofilaments (longitudinal interaction), then laterally interact with each other to form microtubules (lateral interaction). Blue circles represent guanine nucleotide-binding pockets of α- and β-tubulins.

mutations are reported to cause the spectrum of neurologic disorders resulting from neural migration, differentiation, and axon guidance and maintenance abnormalities,[25] demonstrating the importance of αβ-tubulin heterodimers in the nervous system.

In this study, we identified 6 missense *TUBB4A* mutations, 5 of which are novel, in 6 of 7 patients with H-ABC and 2 of 7 patients initially diagnosed with unclassified hypomyelinating leukoencephalopathy. Of the patients with H-ABC, all 6 patients with *TUBB4A* mutations showed typical H-ABC, supporting that H-ABC is a distinct disease entity caused by *TUBB4A* abnormality. We did not detect any *TUBB4A* mutations in one patient with atypical H-ABC. This may be because this patient has a clinically similar, but different disease, possibly caused by a different mutated gene.

We report a *TUBB4A* mutation in 2 patients with preserved basal ganglia. Their brain MRI findings are similar to patients with *POLR3A* or *POLR3B* mutations, rather than H-ABC. However, it is notable that both patients showed apparent extrapyramidal signs, to suggest functional impairment. Accompanying extrapyramidal features are extremely atypical in patients with either *POLR3A* or *POLR3B* mutations.[9,11] Furthermore, comparing these 2 patients with other typical H-ABC patients with *TUBB4A* mutations, patients with minimal basal ganglia atrophy tend to have a milder clinical course. Both patients have a recurrent missense mutation, c.1228G>A (p.Glu410Lys). Based on our 3-dimensional modeling analysis, the Glu410Lys mutation is predicted to directly impair motor protein and/or MAP interactions with microtubules, while the other mutations identified in patients with typical H-ABC may affect longitudinal interactions for maintaining αβ-tubulin heterodimerization/polymerization. Different effects of the *TUBB4A* mutations on tubulin function may lead to this phenotypic variation. Supporting this hypothesis, the p.Glu410Lys mutation in *TUBB3*, which also directly alters a kinesin motor protein binding site in β-tubulin isotype 3, demonstrates clinically distinct features compared with the other mutations.[30] Therefore, the p.Glu410Lys mutation in *TUBB4A* may contribute to the milder end of the phenotypic spectrum of *TUBB4A* mutations. Additional patients with *TUBB4A* mutations are needed to clinically confirm mutational consequences.

Another important finding is that one of the patients with H-ABC had a p.Arg2Gln mutation, since the p.Arg2Gly mutation has recently been identified in patients from a large DYT4 family.[18,19] DYT4 was described in 1985 in an Australian family that had emigrated from England as whispering dysphonia and generalized dystonia. To date, no other pedigrees

Figure 3 Brain MRI of patients with *TUBB4A* mutations

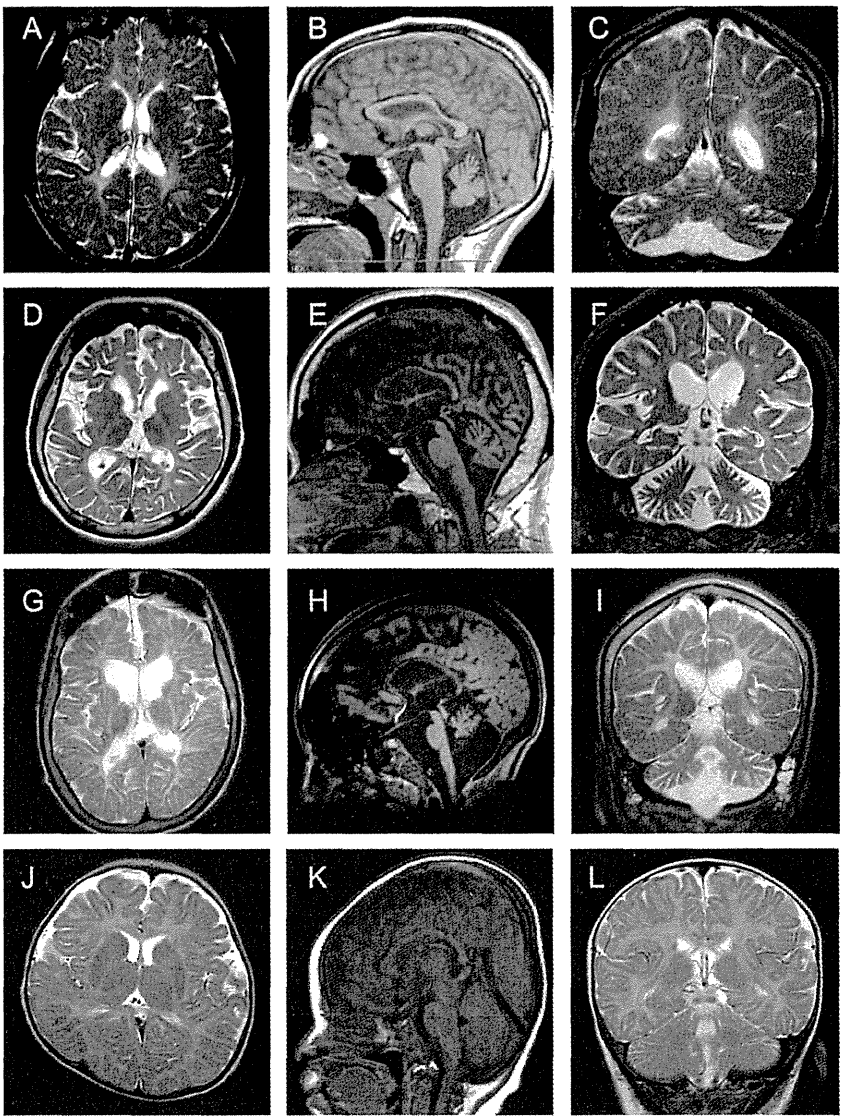


Axial T2-weighted (A, D, G, J), sagittal T1-weighted (B, E, H, K), and coronal T2-weighted (C, F, I, L) images. Patient 1 at 14 years of age (A); patient 1 at 16 years (B, C); patient 2 at 38 years (D–F); patient 3 at 13 years (G–I); and patient 8 at 7 months of age (J–L). All patients show diffuse cerebral white matter hypomyelination with normal (J), mildly reduced (A), or considerably reduced (D, G) white matter volumes. In patient 1, cerebral white matter hypomyelination is unchanged, comparing at 14 (A) and 16 (B, C) years of age. In patient 1, the putamen and the head of the caudate nucleus are normal in size (A). In patient 2, minimal putamen atrophy cannot be excluded (D). The putamen and the head of the caudate nucleus are small or hardly recognizable in patient 3 (G). In patient 8, the putamen is slightly small compared with a healthy control at the same age (J). The globus pallidus and thalamus are normal in size (A, D, G, J). Atrophy of the cerebellar vermis and hemisphere, and corpus callosum was variably observed in 4 patients, but not patient 8 (B, C, E, F, H, I, K, L).

with this phenotype have been reported worldwide.[18] The symptoms typically emerge in the third decade, following a highly penetrant, autosomal dominant mode of inheritance.[31] Brain MRI demonstrates normal structural findings. Arg2 resides within the autoregulatory MREI domain of β-tubulin 4A, which is necessary for autoregulation of the β-tubulin messenger RNA transcript. Site-directed mutagenesis shows that any Arg2 substitution leads to loss of autoregulated instability and increased mutant tubulin subunit levels.[32] Thus, mutations in the MREI domain have been assumed to cause DYT4 rather than H-ABC, because of the different impact on *TUBB4A*.[17] However, our study shows that mutations in the MREI domain can also cause the H-ABC phenotype. The phenotypic difference between the p.Arg2Gly and p.Arg2Gln mutations remains unsolved. Because DYT4 is an extremely rare

syndrome that has only been described in one large pedigree so far, patients of the family may have another modifying factor(s) to spare cerebral white matter abnormalities.

Diffuse hypomyelination syndromes are a heterogeneous group of disorders with overlapping clinical features. Currently, they are categorized based on brain MRI findings, which is very useful in clinical practice. Basal ganglia atrophy specifically distinguishes H-ABC from other hypomyelination disorders. Our study shows that *TUBB4A* mutations associate not only with the typical H-ABC cases but also with some hypomyelinating patients with retained basal ganglia, although notably all patients with *TUBB4A* mutations have extrapyramidal features in common. Our study implies that *TUBB4A* may cause hypomyelinating leukoencephalopathies with either a morphologically or a functionally impaired basal ganglia. Extrapyramidal features may be a key for clinicians to examine *TUBB4A* mutations in genetically unsolved hypomyelinating leukoencephalopathies.

## AUTHOR CONTRIBUTIONS

Satoko Miyatake: genetic and clinical data analysis, data interpretation, and drafting/revising of the manuscript. Hitoshi Osaka: clinical data analysis and sample collection. Masaaki Shiina: structural data analysis. Masayuki Sasaki, Jun-ichi Takanashi, Kazuhiro Haginoya, Takahito Wada, Masafumi Morimoto, Naoki Ando, and Yoji Ikuta: clinical data analysis and sample collection. Mitsuko Nakashima, Yoshinori Tsurusaki, and Noriko Miyake: genetic data analysis. Kazuhiro Ogata: structural data analysis. Naomichi Matsumoto: study concept and design, data interpretation, and drafting/revising of the manuscript. Hirotomo Saitsu: study concept and design, genetic data analysis, data interpretation, and drafting/revising of the manuscript.


## ACKNOWLEDGMENT

The authors thank all of the participants for their cooperation in this research, and Dr. K. Nishiyama, Ms. K. Takabe, Mr. T. Miyama, Ms. A. Narita, Ms. N. Watanabe, and Ms. S. Sugimoto, from the Department of Human Genetics, Yokohama City University Graduate School of Medicine, for their technical assistance.

## STUDY FUNDING

Supported by the Ministry of Health, Labour and Welfare of Japan; the Japan Society for the Promotion of Science (a Grant-in-Aid for Scientific Research [B] [25293085, 25293235]; and a Grant-in-Aid for Scientific Research [A] [13313587]); the Takeda Science Foundation; the fund for Creation of Innovation Centers for Advanced Interdisciplinary Research Areas Program in the Project for Developing Innovation Systems; the Strategic Research Program for Brain Sciences (11105137); and a Grant-in-Aid for Scientific Research on Innovative Areas (Transcription Cycle) from the Ministry of Education, Culture, Sports, Science and Technology of Japan (12024421).

## DISCLOSURE

S. Miyatake is funded by research grants from the Yokohama Foundation for Advancement of Medical Science. H. Osaka is funded by research grants from the Ministry of Health, Labour and Welfare of Japan (Research on Rare and Intractable Diseases [H24-Nanchitou-Ippan-072]). M. Shiina and M. Sasaki report no disclosures relevant to the manuscript. J. Takanashi is funded by research grants from the Ministry of Health, Labour and Welfare of Japan (Research on Rare and Intractable Diseases [H24-Nanchitou-Ippan-072]). K. Haginoya, T. Wada, M. Morimoto, N. Ando, Y. Ikuta, M. Nakashima, and Y. Tsurusaki report no disclosures relevant to the manuscript. N. Miyake is funded by research grants from the Ministry of Health, Labour and Welfare of Japan, a Grant-in-Aid for Scientific Research (B) from the Japan Society for the Promotion of Science, and a research grant from the Takeda Science Foundation. K. Ogata is supported by a Grant-in-Aid for Scientific Research on Innovative Areas (Transcription Cycle) from the Ministry of Education, Culture, Sports, Science and Technology of Japan. N. Matsumoto is supported by grants from the Ministry of Health, Labour and Welfare of Japan, a Grant-in-Aid for Scientific Research (A) from the Japan Society for the Promotion of Science, the Takeda Science Foundation, the fund for Creation of Innovation Centers for Advanced Interdisciplinary Research Areas Program in the Project for Developing Innovation Systems, the Strategic Research Program for Brain Sciences, and a Grant-in-Aid for Scientific Research on Innovative Areas (Transcription Cycle) from the Ministry of Education, Culture, Sports, Science and Technology of Japan. H. Saitsu is funded by research grants from a Grant-in-Aid for Scientific Research (B) from the Japan Society for the Promotion of Science, and a research grant from the Takeda Science Foundation. Go to Neurology.org for full disclosures.

*Received October 10, 2013. Accepted in final form March 20, 2014.*


## REFERENCES


1. Schiffmann R, van der Knaap MS. Invited article: an MRI-based approach to the diagnosis of white matter disorders. Neurology 2009;72:750–759.
2. Steenweg ME, Vanderver A, Blaser S, et al. Magnetic resonance imaging pattern recognition in hypomyelinating disorders. Brain 2010;133:2971–2982.
3. Wolf NI, Harting I, Boltshauser E, et al. Leukoencephalopathy with ataxia, hypodontia, and hypomyelination. Neurology 2005;64:1461–1464.
4. Timmons M, Tsokos M, Asab MA, et al. Peripheral and central hypomyelination with hypogonadotropic hypogonadism and hypodontia. Neurology 2006;67:2066–2069.
5. Vazquez-Lopez M, Ruiz-Martin Y, de Castro-Castro P, Garzo-Fernandez C, Martin-del Valle F, Marquez-de la Plata L. Central hypomyelination, hypogonadotrophic hypogonadism and hypodontia: a new leukodystrophy [in Spanish]. Rev Neurol 2008;47:204–208.
6. Bernard G, Thiffault I, Tetreault M, et al. Tremor-ataxia with central hypomyelination (TACH) leukodystrophy maps to chromosome 10q22.3-10q23.31. Neurogenetics 2010;11:457–464.
7. Atrouni S, Daraze A, Tamraz J, Cassia A, Caillaud C, Megarbane A. Leukodystrophy associated with oligodontia in a large inbred family: fortuitous association or new entity? Am J Med Genet A 2003;118A:76–81.
8. Chouery E, Delague V, Jalkh N, et al. A whole-genome scan in a large family with leukodystrophy and oligodontia reveals linkage to 10q22. Neurogenetics 2011;12:73–78.
9. Sasaki M, Takanashi J, Tada H, Sakuma H, Furushima W, Sato N. Diffuse cerebral hypomyelination with cerebellar atrophy and hypoplasia of the corpus callosum. Brain Dev 2009;31:582–587.
10. Bernard G, Chouery E, Putorti ML, et al. Mutations of POLR3A encoding a catalytic subunit of RNA polymerase Pol III cause a recessive hypomyelinating leukodystrophy. Am J Hum Genet 2011;89:415–423.
11. Saitsu H, Osaka H, Sasaki M, et al. Mutations in POLR3A and POLR3B encoding RNA polymerase III subunits cause an autosomal-recessive hypomyelinating leukoencephalopathy. Am J Hum Genet 2011;89:644–651.
12. Tetreault M, Choquet K, Orcesi S, et al. Recessive mutations in POLR3B, encoding the second largest subunit of Pol III, cause a rare hypomyelinating leukodystrophy. Am J Hum Genet 2011;89:652–655.

13. Potic A, Brais B, Choquet K, Schiffmann R, Bernard G. 4H syndrome with late-onset growth hormone deficiency caused by POLR3A mutations. Arch Neurol 2012;69: 920–923.
14. Daoud H, Tetreault M, Gibson W, et al. Mutations in POLR3A and POLR3B are a major cause of hypomyelinating leukodystrophies with or without dental abnormalities and/or hypogonadotropic hypogonadism. J Med Genet 2013;50:194–197.
15. van der Knaap MS, Naidu S, Pouwels PJ, et al. New syndrome characterized by hypomyelination with atrophy of the basal ganglia and cerebellum. AJNR Am J Neuroradiol 2002;23:1466–1474.
16. van der Knaap MS, Linnankivi T, Paetau A, et al. Hypomyelination with atrophy of the basal ganglia and cerebellum: follow-up and pathology. Neurology 2007;69: 166–171.
17. Simons C, Wolf NI, McNeil N, et al. A de novo mutation in the beta-tubulin gene TUBB4A results in the leukoencephalopathy hypomyelination with atrophy of the basal ganglia and cerebellum. Am J Hum Genet 2013;92: 767–773.
18. Hersheson J, Mencacci NE, Davis M, et al. Mutations in the autoregulatory domain of beta-tubulin 4a cause hereditary dystonia. Ann Neurol 2013;73:546–553.
19. Lohmann K, Wilcox RA, Winkler S, et al. Whispering dysphonia (DYT4 dystonia) is caused by a mutation in the TUBB4 gene. Ann Neurol 2013;73:537–545.
20. Lowe J, Li H, Downing KH, Nogales E. Refined structure of alpha beta-tubulin at 3.5 Å resolution. J Mol Biol 2001; 313:1045–1057.
21. Uchimura S, Oguchi Y, Katsuki M, et al. Identification of a strong binding site for kinesin on the microtubule using mutant analysis of tubulin. EMBO J 2006;25:5932–5941.
22. Al-Bassam J, Ozer RS, Safer D, Halpain S, Milligan RA. MAP2 and tau bind longitudinally along the outer ridges of microtubule protofilaments. J Cell Biol 2002;157: 1187–1196.
23. Nawrotek A, Knossow M, Gigant B. The determinants that govern microtubule assembly from the atomic structure of GTP-tubulin. J Mol Biol 2011;412:35–42.
24. Nogales E, Whittaker M, Milligan RA, Downing KH. High-resolution model of the microtubule. Cell 1999; 96:79–88.
25. Tischfield MA, Cederquist GY, Gupta ML Jr, Engle EC. Phenotypic spectrum of the tubulin-related disorders and functional implications of disease-causing mutations. Curr Opin Genet Dev 2011;21:286–294.
26. Wakusawa K, Haginoya K, Kitamura T, et al. Effective treatment with levodopa and carbidopa for hypomyelination with atrophy of the basal ganglia and cerebellum. Tohoku J Exp Med 2006;209:163–167.
27. Hattori A, Ando N, Fujimoto S, Kobayashi S, Ishikawa T, Togari H. A boy with hypomyelination with atrophy of the basal ganglia and cerebellum [in Japanese]. No To Hattatsu 2010;42:42–44.
28. Leandro-Garcia LJ, Leskela S, Landa I, et al. Tumoral and tissue-specific expression of the major human beta-tubulin isotypes. Cytoskeleton 2010;67:214–223.
29. Sullivan KF, Cleveland DW. Sequence of a highly divergent beta tubulin gene reveals regional heterogeneity in the beta tubulin polypeptide. J Cell Biol 1984;99:1754–1760.
30. Chew S, Balasubramanian R, Chan WM, et al. A novel syndrome caused by the E410K amino acid substitution in the neuronal beta-tubulin isotype 3. Brain 2013;136: 522–535.
31. Parker N. Hereditary whispering dysphonia. J Neurol Neurosurg Psychiatry 1985;48:218–224.
32. Yen TJ, Machlin PS, Cleveland DW. Autoregulated instability of beta-tubulin mRNAs by recognition of the nascent amino terminus of beta-tubulin. Nature 1988;334: 580–585.

# *PIGA* mutations cause early-onset epileptic encephalopathies and distinctive features

Mitsuhiro Kato, MD, PhD*
Hirotomo Saitsu, MD, PhD*
Yoshiko Murakami, MD, PhD*
Kenjiro Kikuchi, MD
Shuei Watanabe, MD
Mizue Iai, MD
Kazushi Miya, MD
Ryuki Matsuura, MD
Rumiko Takayama, MD
Chihiro Ohba, MD
Mitsuko Nakashima, MD, PhD
Yoshinori Tsurusaki, PhD
Noriko Miyake, MD, PhD
Shin-ichiro Hamano, MD
Hitoshi Osaka, MD, PhD
Kiyoshi Hayasaka, MD, PhD
Taroh Kinoshita, PhD
Naomichi Matsumoto, MD, PhD

## ABSTRACT

**Objective:** To investigate the clinical spectrum caused by mutations in *PIGA* at Xp22.2, which is involved in the biosynthesis of the glycosylphosphatidylinositol (GPI) anchor, among patients with early-onset epileptic encephalopathies (EOEEs).

**Methods:** Whole-exome sequencing was performed as a comprehensive genetic analysis for a cohort of 172 patients with EOEEs including early myoclonic encephalopathy, Ohtahara syndrome, and West syndrome, and *PIGA* mutations were carefully investigated.

**Results:** We identified 4 *PIGA* mutations in probands showing early myoclonic encephalopathy, West syndrome, or unclassified EOEE. Flow cytometry of blood granulocytes from patients demonstrated reduced expression of GPI-anchored proteins. Expression of GPI-anchored proteins in *PIGA*-deficient JY5 cells was only partially or hardly restored by transient expression of PIGA mutants with a weak TATA box promoter, indicating a variable loss of PIGA activity. The phenotypic consequences of *PIGA* mutations can be classified into 2 types, severe and less severe, which correlate with the degree of PIGA activity reduction caused by the mutations. Severe forms involved myoclonus and asymmetrical suppression bursts on EEG, multiple anomalies with a dysmorphic face, and delayed myelination with restricted diffusion patterns in specific areas. The less severe form presented with intellectual disability and treatable seizures without facial dysmorphism.

**Conclusions:** Our study confirmed that *PIGA* mutations are one genetic cause of EOEE, suggesting that GPI-anchor deficiencies may be an underlying cause of EOEE. ***Neurology*® 2014;82:1587–1596**

## GLOSSARY

**ADC** = apparent diffusion coefficient; **cDNA** = complementary DNA; **DWI** = diffusion-weighted image; **EME** = early myoclonic encephalopathy; **EOEE** = early-onset epileptic encephalopathy; **GPI** = glycosylphosphatidylinositol; **GPI-AP** = glycosylphosphatidylinositol-anchored protein; **OS** = Ohtahara syndrome; **WES** = whole-exome sequencing.

Early-onset epileptic encephalopathies (EOEEs) present with developmental impairment and disastrous seizures starting in early infancy with a mode of age dependency. Ohtahara syndrome (OS) and early myoclonic encephalopathy (EME), both of which show a distinctive EEG finding called suppression-burst pattern, are neonatal EOEEs. Genetic approaches have revealed some of the genes that are mutated in EOEEs. For instance, *ARX*, *STXBP1*, *CASK*, *KCNQ2*, and *SCN2A* are mutated in OS,[1–5] while *ARX*, *CDKL5*, and *SPTAN1* mutations cause West syndrome or infantile spasms.[6–8]

Mutations in 8 genes (*PIGA*, *PIGM*, *PIGN*, *PIGV*, *PIGL*, *PIGO*, *PIGT*, and *PGAP2*) involved in the biosynthesis of the glycosylphosphatidylinositol (GPI) anchor, a glycolipid structure embedded in the plasma membrane that attaches to hundreds of cell-surface proteins, have been identified in patients with a variety of multiple congenital anomalies, intellectual disability, and epileptic seizures.[9–16] Somatic mutations of *PIGA* at Xp22.2, which is involved in

Correspondence to Dr. Kato: mkato@med.id.yamagata-u.ac.jp or Dr. Saitsu: hsaitsu@yokohama-cu.ac.jp

**Supplemental data at Neurology.org**

*These authors contributed equally to this work.

From the Department of Pediatrics (M.K., K.H.), Yamagata University Faculty of Medicine, Yamagata; Department of Human Genetics (H.S., C.O., M.N., Y.T., N. Miyake, N. Matsumoto), Yokohama City University Graduate School of Medicine, Yokohama; Department of Immunoregulation (Y.M., T.K.), Research Institute for Microbial Diseases, and WPI Immunology Frontier Research Center, Osaka University, Suita; Division of Neurology (K.K., R.M., S.-i.H.), Saitama Children's Medical Center, Saitama; Division of Neurology (S.W.), Miyagi Children's Hospital, Sendai; Division of Neurology (M.I., H.O.), Clinical Research Institute, Kanagawa Children's Medical Center, Yokohama; Department of Pediatrics (K.M.), Graduate School of Medicine and Pharmaceutical Sciences, University of Toyama; Department of Pediatrics (R.T.), Aomori Prefectural Central Hospital, Aomori; and Department of Pediatrics (H.O.), Jichi Medical School, Tochigi, Japan.

Go to Neurology.org for full disclosures. Funding information and disclosures deemed relevant by the authors, if any, are provided at the end of the article.

the first step of the GPI biosynthesis, are responsible for paroxysmal nocturnal hemoglobinuria, and its germline mutation, were recently identified in a family with multiple congenital anomalies, neonatal seizures, and a poor prognosis.[11] At least 2 of 3 patients in this family showed severe myoclonic seizures with suppression bursts on EEG, strongly suggesting EME. The known mutations in EME prompted us to investigate *PIGA* in the EOEE patient cohort including EME and OS. We identified *PIGA* mutations in 5 patients from 4 families with EOEEs and present the clinical phenotypes of the patients and functional effects of the mutations in this study.

## METHODS

**Patients.** A total of 172 patients with EOEEs (2 with EME, 50 with OS, 50 with West syndrome or infantile spasms, 7 with malignant migrating partial seizures in infancy, and 63 with unclassified epileptic encephalopathy with an age at onset of <1 year; 90 male and 82 female patients) were analyzed by whole-exome sequencing (WES), and *PIGA* mutations were carefully investigated using WES data.

Patients had been mainly enrolled in the Japanese collaborative study for EOEE since 2003. The diagnosis was made based on clinical features and characteristic EEG patterns. Patients with mutations in *STXBP1*, *ARX*, *KCNQ2*, *SCN1A*, *SCN2A*, *KCNT1*, *CDKL5*, *CASK*, or *MECP2*, which were detected by high-resolution melting analysis, target capture analysis, direct sequencing analysis, or WES, were excluded from the study.

**Whole-exome sequencing.** Patient and parental genomic DNA was obtained from peripheral blood leukocytes using standard methods. DNA was captured using the SureSelectXT Human All Exon Kit (v4 or v5; Agilent Technologies, Santa Clara, CA) and sequenced on an Illumina HiSeq2000 (Illumina, San Diego, CA) with 101–base pair paired-end reads. Image analysis and base calling were performed using sequence control software real-time analysis and CASAVA software v1.8 (Illumina). Exome data processing, variant calling, and variant annotation were performed as previously described.[17–19] All novel mutations in *PIGA* were verified using Sanger sequencing.

**Fluorescence-activated cell sorting analysis.** Surface expression of GPI-anchored proteins (GPI-APs) was determined by staining cells with Alexa 488–conjugated inactivated aerolysin (FLAER; Protox Biotech, Victoria, Canada) and appropriate primary antibodies, namely, mouse anti-CD59 (5H8), DAF (IA10), CD16 (3G8), CD24 (ML5), and CD48 (BJ40), followed by a phycoerythrin-conjugated anti-mouse immunoglobulin G antibody (3G8, ML5, BJ40, and secondary antibodies; BD Biosciences, Franklin Lakes, NJ). Cells were analyzed by flow cytometry (Cant II; BD Biosciences).

**Functional analysis using *PIGA*-deficient B lymphoblastoid cells (JY5).** FLAG-tagged human *PIGA* complementary DNA (cDNA) and mutant cDNAs, generated by site-directed mutagenesis, were subcloned into the pMEoriP vector, a strong promoter (SRα)-driven vector or pTAoriP, a weak TATA box promoter-driven vector. Plasmid DNA was transfected by electroporation into *PIGA*-deficient JY5 cells. Expression of GPI-APs was analyzed by fluorescence-activated cell sorting. PIGA protein levels in transfected cells were determined by Western blotting using an anti-FLAG antibody (M2; Sigma, St. Louis, MO).

**Standard protocol approvals, registrations, and patient consents.** The experimental protocols were approved by the institutional review boards for ethical issues of Yamagata University Faculty of Medicine, Yokohama City University School of Medicine, and Osaka University, Japan. Written informed consent was obtained from all individuals and/or their families in compliance with relevant Japanese regulations. Permission for publishing photographs was also obtained from the parents.

## RESULTS

**Identification of *PIGA* mutations.** No mutations were found in *SLC25A22*, which had been reported in a family of EME.[20] We identified 4 hemizygous *PIGA* mutations in 3 sporadic patients and 2 siblings with EOEE. One mutation (c.1234C>T [p.R412X]) had previously been reported,[11] while the other 3 were novel missense mutations (c.230G>T [p.R77L], c.616A>T [p.I206F], and c.355C>T [p.R119W]). DNA from the mother of patient 1 (p.R412X) was unavailable. Three missense mutations were maternally inherited. All mutations were absent from the 6,500 exomes of the National Heart, Lung, and Blood Institute exome project and our 573 in-house control exomes (281 male and 292 female patients). All 4 mutations occurred at evolutionarily conserved amino acids (figure 1A) and were predicted to be highly damaging to the protein structure by SIFT, PolyPhen-2, and MutationTaster (table e-1 on the *Neurology*® Web site at Neurology.org), which supported their pathogenicity.

**Clinical features of patients with the *PIGA* mutation.** The clinical information of individuals with a *PIGA* mutation is summarized in table 1, and their facial appearances and representative brain images are shown in figures 1 and 2, respectively. EEG findings (figure e-1) and detailed case reports (appendix e-1) are available in supplemental data. Two patients were associated with polyhydramnios. Birth weight and length were normal in 3 patients (patients 2, 3, and 5) who were born at term, but the other 2 who were born at preterm showed higher (patient 1) or lower (patient 4) birth weights than normal. Three patients with the severe phenotype (patients 1, 2, and 5) showed facial dysmorphisms (figure 1, B and C), including a depressed nasal bridge, short anteverted nose, downturned corners of the mouth, and high arched palate. Patient 1 also showed bilateral vesicoureteral reflux of the most severe grade V. In addition, brain MRI demonstrated a thin corpus callosum and delayed myelination in these patients. Of interest, abnormally high signals on diffusion-weighted images (DWIs) and low signals on the apparent diffusion coefficient (ADC) map at the brainstem, basal ganglia, thalamus, and deep white matter were found in patients 1, 2, and 5 (figure 2, A–D and M–Q). By

**Figure 1** *PIGA* mutations in patients with epileptic encephalopathy and dysmorphic features

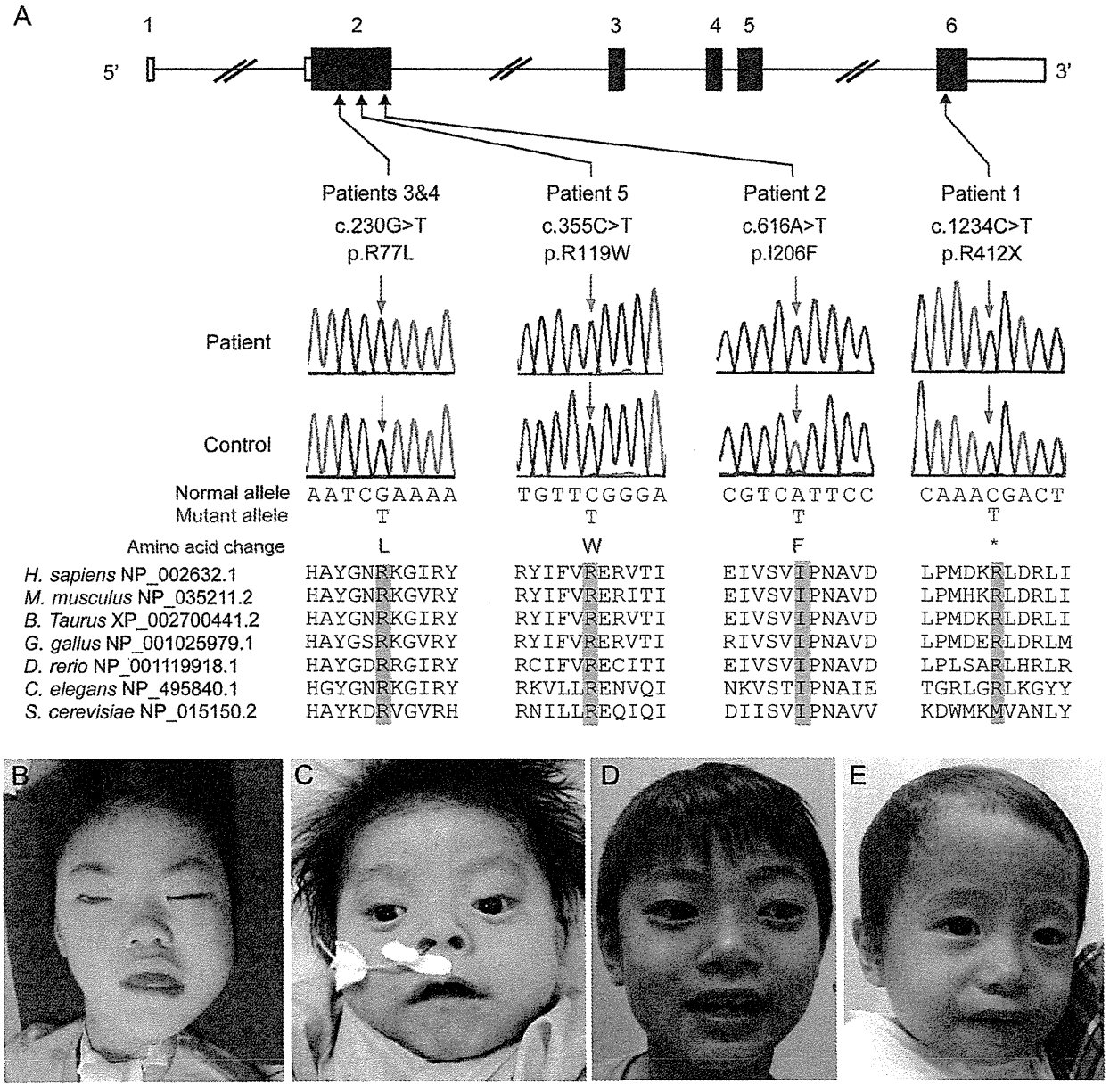


(A) Schematic presentation of *PIGA* genomic structure. Mutations are indicated based on the transcript variant 1 (GenBank accession number, NM_002641.3). Untranslated regions and coding regions are shown as white and black rectangles, respectively. All mutations occurred at evolutionarily conserved amino acids. Orthologous sequences were aligned using the CLUSTALW Web site. (B–E) Facial appearance of patients 2, 3, 4, and 5. Both patients 2 (B) and 5 (C) show distinct facial features, such as upslanting palpebral fissures, depressed nasal bridge, short anteverted nose, triangular mouth with downturned corners, and high arched palate, compared with patients 3 (D) and 4 (E) with no dysmorphic facial features.

contrast, 2 brothers with a less severe phenotype (patients 3 and 4) showed neither dysmorphic signs nor abnormalities in brain MRI (figure 2, E–L).

The first seizures started between 1 and 7 months of age, and tonic or myoclonic seizures occurred in all patients. Seizures of patients 1, 2, and 5 were refractory to antiepileptic medications, but topiramate was effective for the seizures of patient 3. The initial EEG showed a suppression burst in patient 1; patients 2 and 5 first demonstrated hypsarrhythmia, followed by a symmetrical or asymmetrical suppression burst later (figure e-1). Serum alkaline phosphatase levels were elevated in patients 2 and 5. No patients showed anemia or hemoglobinuria. All patients showed profound intellectual disability, and patients 1, 2, and 5 were bedridden with severe motor disturbance.

**Flow cytometry.** We analyzed the surface expression of various GPI-APs on patient granulocytes using flow

**Table 1** Clinical summary of patients with a *PIGA* mutation

| | Patients | | | | | | |
|---|---|---|---|---|---|---|---|
| | IV-2 | IV-4 | 1 | 2 | 3 | 4 | 5 |
| **Familial or sporadic** | Familial or sporadic | Familial (brother) | Sporadic | Sporadic | Familial (proband) | Familial (brother) | Sporadic |
| **Mutation** | c.1234C>T (p.R412X) | c.1234C>T (p.R412X) | c.1234C>T (p.R412X) | c.616A>T (p.I206F) | c.230G>T (p.R77L) | c.230G>T (p.R77L) | c.355C>T (p.R119W) |
| **Current age** | Died at 11 wk | Died at 10 wk | 6 y | 10 y | 8 y | 18 mo | 15 mo |
| **Sex** | M | M | M | M | M | M | M |
| **Clinical diagnosis** | | | Ohtahara syndrome, early myoclonic encephalopathy, Schinzel-Giedion syndrome | West syndrome with hypomyelination | Early-onset epileptic encephalopathy | Early-onset epileptic encephalopathy | West syndrome |
| **Polyhydramnios** | – | + | + | – | – | – | + |
| **Gestation, wk** | Full term | 35 | 33 | 40 | 38 | 36 | 39 |
| **Birth weight, g** | 3,540 | 3,500 | 2,857 | 3,566 | 2,715 | 1,896 | 3,468 |
| **Birth length, cm** | 53.5 | 48 | 42.0 | 50 | 50 | ND | 47 |
| **Birth head circumference, cm** | 37 | 35.5 | 33.2 | ND | 32.5 | ND | 33.5 |
| **Facial dysmorphism** | + | + | + | + | – | – | + |
| **Vesicoureteral reflux** | + | ND | + | ND | – | – | ND |
| **Joint contractures** | + | + | + | + | – | – | – |
| **Hypotonia** | + | + | + | – | – | – | + |
| **Hyperreflexia** | + | + | ND | – | – | – | + |
| **Seizure onset** | Neonate | Neonate | 1 mo | 3 mo | 7 mo | 7 mo | 3 mo |
| **Seizure types** | Myoclonic | Severe myoclonic | Tonic seizures followed by frequent myoclonus | Myoclonus or epileptic spasm-like movement | Tonic seizures, secondarily generalized seizures | Tonic or clonic | Myoclonic seizures, tonic spasms |
| **EEG findings** | Suppression burst | Suppression burst | Suppression burst at neonatal period | Hypsarrhythmia at 3 mo, periodic bursts of multifocal epileptic discharges similar to suppression-burst pattern at 10 y | Normal at 7 mo, irregular spike and slow wave and multifocal spikes at 2 and 5 y | Normal at 7 mo | Hypsarrhythmia at 3 mo, suppression burst at 5 mo |
| **Seizure prognosis** | Intractable | Intractable | Intractable | Intractable | Seizure-free at 3 y with TPM | Seizure-free at 15 mo | Intractable |
| **Development** | Early death | Early death | Hypotonic quadriplegia, profound intellectual disability | Spastic quadriplegia, profound intellectual disability | Profound intellectual disability with autism, but no motor disturbance | Moderate intellectual disability, but no motor disturbance | Hypotonic quadriplegia, profound intellectual disability |
| **Thin corpus callosum** | + | + | + | + | – | – | + (at 9 mo) |
| **White matter immaturity** | + | + | + | + | – | – | + (at 9 mo) |
| **Restricted diffusion pattern** | ND | ND | + | + | – | – | + |
| **Elevated serum alkaline phosphatase** | ND | + | ND | + | – | – | + |

Abbreviations: ND = not determined; TPM = topiramate.

Figure 2 Brain MRIs of patients with *PIGA* mutations

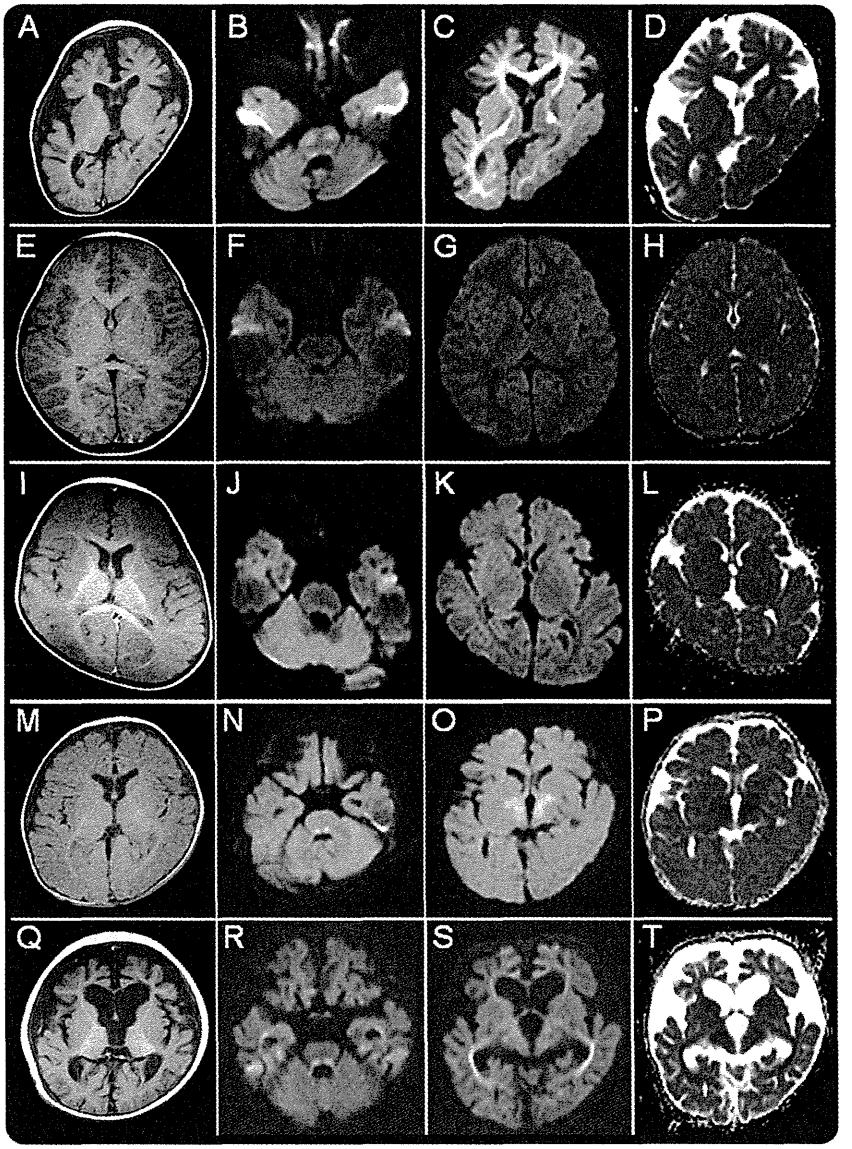


MRIs of patient 2 at 6 months (A) and 7 years (B–D), patient 3 at 3 years (E–H), patient 4 at 7 months (I–L), and patient 5 at 3 months (M–P) and 9 months (Q–T) of age. Left panels (A, E, I, M, Q) show axial T1-weighted images, the 2 middle panels (B, C, F, G, J, K, N, O, R, S) show axial diffusion-weighted images (DWIs), and right panels (D, H, L, P, T) show apparent diffusion coefficient (ADC) maps. Patient 2 and patient 5 at 9 months show cortical atrophy and enlarged ventricles. Note the high signals on DWI in the pontine tegmentum and deep white matter, particularly the optic radiation, of patients 2 and 5 in accordance with their age. The ADC map demonstrated decreased ADC within the same lesion. Patients 3 and 4 show normal images.

cytometry (figure 3). In all 5 patients, the surface expression of CD16 was severely decreased (from 5% to 15% of normal levels). Patient 1, with the most severe clinical symptoms, had a tendency to show reduced expression of other GPI-APs, such as CD24 and FLAER (figure 4A). Because *PIGA* is an X-linked gene and one allele is inactivated during early embryogenesis in female patients, patient mothers would be functionally mosaic for GPI-AP expression. Granulocytes from the mother of patients 3 and 4 showed a significantly decreased expression of CD16 (figure e-2, upper panels), whereas those from the mother of patient 5 showed normal expression (figure e-2, lower panels). The mothers appeared to have no neurologic disorder, suggesting that GPI-sufficient cells may preferentially proliferate in the brain during early embryogenesis.

**Functional analysis.** *PIGA* cDNAs bearing patient mutations were functionally analyzed by transfecting them into *PIGA*-deficient B lymphoblastoid cells (JY5) and measuring the surface expression of GPI-APs.

Figure 3 Flow cytometry of granulocytes

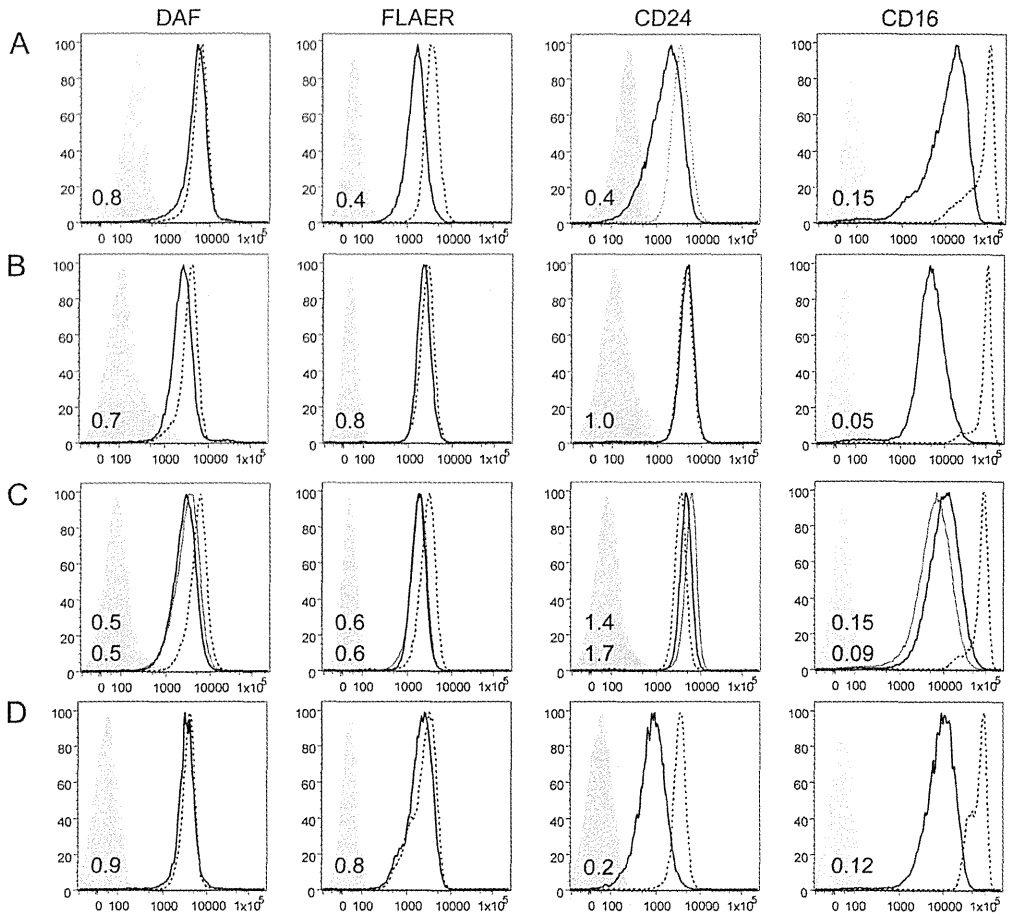


Flow cytometry of patient 1 (R412X) (A), patient 2 (I206F) (B), patients 3 and 4 (2 brothers, R77L) (C), and patient 5 (R119W) (D). In all families, the surface expression of various glycosylphosphatidylinositol-anchored proteins on patient granulocytes (solid lines; patients 3 and 4 are shown in C as thin and thick lines, respectively) was severely decreased compared with the normal control (dotted lines). Light shadows represent isotype controls. Mean fluorescent intensities of each sample against a normal control are shown in each panel (upper, patient 4; lower, patient 3 in C).

When strong promoter (SRα)-driven constructs were used, R412X mutant cDNA completely restored the surface expression of CD59, DAF, and CD48, whereas R412 truncated cDNA had no activity (figure 4A), suggesting that a small amount of full-length PIGA protein was generated by readthrough of a stop codon. When weak promoter-driven constructs (pTA) were used instead, R412X cDNA could not restore the surface expression of GPI-APs, whereas it was completely restored by wild-type cDNA (figure 4B). Similarly, the strong promoter (SRα)-driven I206F and R77L mutant PIGAs completely restored the surface expression of GPI-APs, whereas the weak promoter-driven mutant constructs only partially restored this (figure 4, C–F). Levels of expressed mutant PIGA proteins were similar to or even higher than wild-type levels (figure e-3). A faint band representing full-length PIGA protein harboring R412X could be detected (figure e-3, lane 4), which was consistent with the functional analysis. From these results, we concluded that these mutations affect the PIGA activity leading to inherited GPI deficiency.

**DISCUSSION** We have identified 4 *PIGA* mutations in 172 probands from a variety of EOEE-affected families, such as EME (n = 1), West syndrome (n = 2), and unclassified EOEE in a sibling. Myoclonus and suppression burst on EEG were recognized in 2 patients with West syndrome and the patient with EME in our cohort, as well as the previously reported family.[11] Indeed, myoclonus and suppression burst on EEG appear to be characteristic features for patients with a *PIGA* mutation.

Other clinical features such as polyhydramnios, facial dysmorphism, joint contractures, hypotonia, and severe developmental delay are recurrently seen in patients with *PIGA* mutations. A previous report of 3 patients with the same nonsense mutation,

Figure 4 Functional analysis of the mutant PIGA

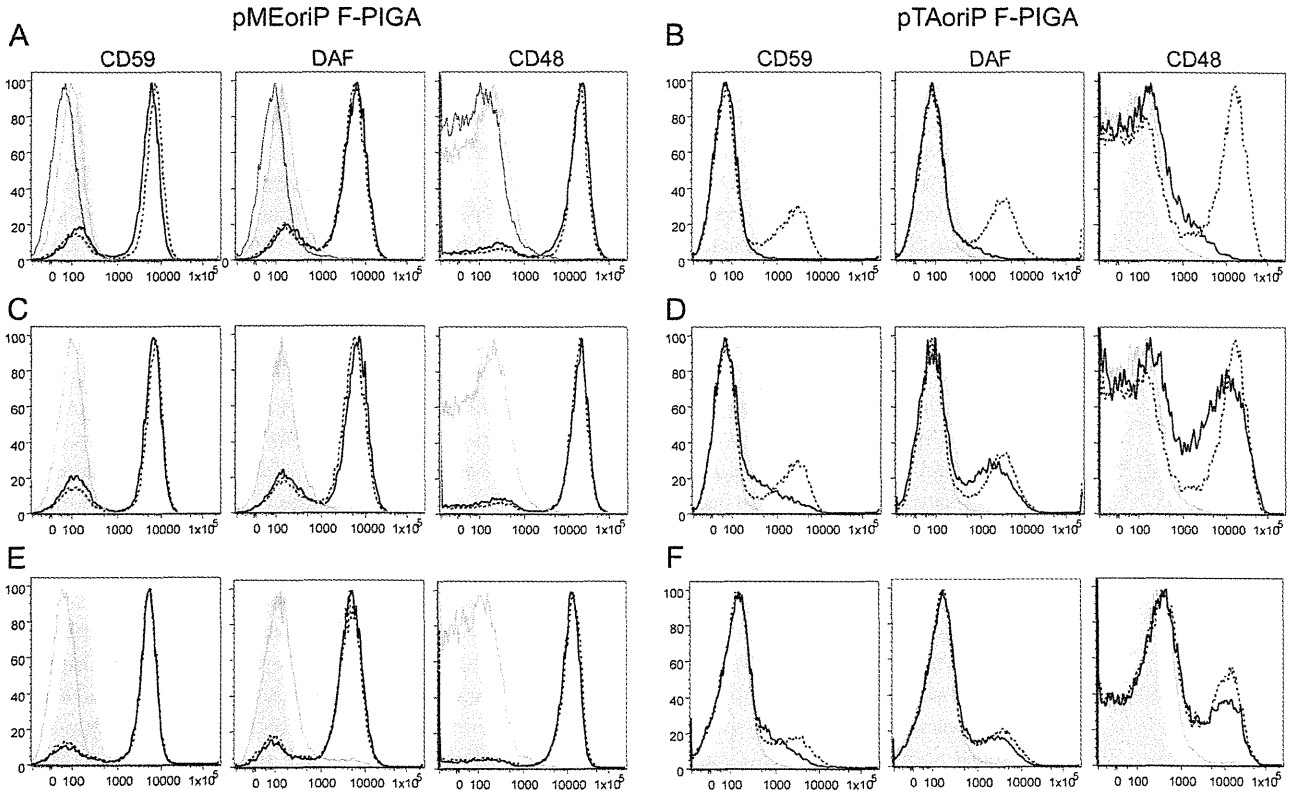


JY5 cells were transiently transfected with pMEoriP (strong SRα promoter-driven, Epstein-Barr [EB] virus origin-containing vector) (panels A, C, and E) or pTAoriP F-PIGA (weak TATA box promoter-driven, EB virus origin-containing vector) (panels B, D, and F) bearing various FLAG-tagged PIGA complementary DNAs. Restoration of the surface expression of CD59, DAF, and CD48 was assessed 2 days later by flow cytometry. Dotted lines represent wild-type PIGA, thick lines represent mutant PIGA, thin lines represent truncated PIGA, and shadows represent isotype controls. (A) Strong promoter-driven R412X PIGA (thick lines) completely rescued the expression of glycosylphosphatidylinositol-anchored proteins (GPI-APs) similar to wild-type PIGA (dotted lines), whereas R412-truncated PIGA (thin lines) had no activity. (B) Weak promoter-driven R412X PIGA (thick lines) did not rescue the surface expression of GPI-APs, whereas wild-type PIGA (dotted lines) did. (C) Strong promoter-driven I206F PIGA (thick lines) completely rescued the expression of GPI-APs similar to wild-type PIGA (dotted lines). (D) Weak promoter-driven I206F PIGA (thick lines) did not rescue the surface expression of GPI-APs, whereas wild-type PIGA (dotted lines) did. (E) Strong promoter-driven R77L PIGA (thick lines) completely rescued the expression of GPI-APs similar to wild-type PIGA (dotted lines). (F) Weak promoter-driven R77L PIGA (thick lines) did not rescue the surface expression of CD59, whereas wild-type PIGA (dotted lines) did.

R412X,[11] as patient 1 in our cohort showed similar or more severe clinical features, such as a large occipitofrontal circumference at birth, early-onset intractable seizures, and severe respiratory failure leading to early death or mechanical ventilation. Complete disruption of the *PIGA* gene results in early embryonic lethality in male mice, while heterozygous female mice have late embryonic lethality, insufficient closure of the neural tube, and a cleft palate.[21] In the present study, a reduced but definite expression of GPI-APs in the granulocytes of patients with R412X and a complete restoration of GPI-AP surface expression by the transfection of R412X mutant cDNA under the control of a strong promoter suggest that small amounts of full-length PIGA protein were generated by the read-through of a stop codon because the cDNA truncated at R412 showed no activity.

The siblings with the *PIGA* p.R77L mutation demonstrated milder clinical symptoms compared with patients with other *PIGA* mutations. They showed neither dysmorphisms nor severe motor disturbance, the onset of their seizures was relatively late, and the findings of their initial EEG and brain MRI were normal. Flow cytometry only revealed a decreased expression of CD16, which contrasts with the more severe phenotype of patient 1 and associated decreased levels of CD16, FLAER, and CD24. According to the functional study using *PIGA*-deficient B lymphoblasts transfected with a weak promoter-driven mutant *PIGA*, the activity of the R77L mutant was higher than that of other mutants. Thus, the phenotype severity appears to correlate with genotype and the residual functional activity of the PIGA protein.

Patients 2 and 5 showed peculiarly high signals on DWI at the specific areas of the brainstem, basal ganglia, thalamus, and deep white matter, particularly the optic radiation as previously reported in patient 1.[22] Although delayed myelination and the volume loss of